PHASE SEPARATED HYDROGEL COATINGS FOR POROUS SCAFFOLDS IN BIOMEDICAL APPLICATIONS

by

AMANDA KURTZ

A THESIS

Presented to the Department of Chemistry and Biochemistry
and the Robert D. Clark Honors College
in partial fulfillment of the requirements for the degree of
Bachelor of Science

April 2023

An Abstract of the Thesis of

Amanda Kurtz for the degree of Bachelor of Science
in the Department of Chemistry and Biochemistry to be taken June 2023

Title: Phase Separated Hydrogel Coatings for Porous Scaffolds in Biomedical Applications

Approved: *Paul Dalton, Ph.D.*
Primary Thesis Advisor

The field of tissue engineering (TE) works to produce artificial replicas of tissues and organs for clinical applications. To achieve this ambitious outcome, TE works at the interface of biology, engineering, and medicine to produce reasonable substitutes. Additive manufacturing (AM), commonly known as 3D printing, allows for the production of porous 3D structures, termed scaffolds, to replace previously 2D models of cell culture study for TE. Within AM, melt electrowriting advances the resolution possible through its unique fabrication of high precision, micron thin fibers. These microfibers are applicable on a biological scale and allow for the formation of highly porous scaffold structures for cell culture studies. The polymer used in this thesis is poly(ε-caprolactone) (PCL) which, with its low melting point, rapid solidification, and biocompatibility, is the gold-standard for MEW. PCL, however, is limited in its efficacy for 3D cell culture due to its hydrophobic nature, resulting in poor cell attachment. A possible solution to this limitation is with a hydrophilic hydrogel coating, such as poly(2-hydroxyethyl methacrylate) (pHEMA). Prior to implementation in TE studies, it must be understood how pHEMA coats these scaffolds and whether this coating interferes with important cell culture techniques. This thesis therefore investigates the relevance of the combination of these two materials from a coating and cell culture standpoint.

Acknowledgements

I would like to thank the many people that helped me through this thesis process and my college career.

Thank you to the Dalton lab for providing me with the opportunity to conduct this research while providing guidance, assistance, and many memories during my two years in the lab. A special thanks to Dr. Paul Dalton for all his guidance in learning the research process and encouraging me to ask questions, Kelly for being my mentor and helping conduct the experiments, and Dr. Naomi Paxton for all her assistance in writing and editing this document. Thanks to the Guldberg lab for allowing me to use their cell culture facilities to complete my research. Finally, I would like to thank the Knight Campus Undergraduate Program for funding my research and providing me with an amazing group of peers.

Thanks to the Clark Honors College for encouraging me to think outside the box with a wide array of unique classes and fantastic professors. A special thanks to Dr. Daphne Gallagher for agreeing to be on my committee and providing advice and wisdom throughout my college career. I would also like to thank Dr. Angela Rovak for being a constant support and mentor throughout college.

Finally, thank you to all the people outside of academia that have supported me through this process. Thank you, Carmen, Cora, Teagan, and Nico, for providing endless support, laughs, and more conversations about STEM than I thought possible. Thank you to my family for supporting me through all the ups and downs of this journey. And finally, Toby Fox for the music that got me through this journey.

Table of Contents

Introduction: Scaffold-based Tissue Engineering 7
- Tissue Engineering 7
- Melt Electrowriting 10
- Project Motivations 14
- Our Approach: Combination of Two Clinically Relevant Materials 16

Chapter 1: pHEMA Hydrogel Coatings 18
- Introduction 18
- Methods 21
  - Scaffold Design and Fabrication 21
  - NaOH Pretreatment 23
  - PHEMA coatings 23
  - Agitated pHEMA coatings 24
  - Image analysis 26
  - Scanning Electron Microscopy 27
- Results and Discussion 27
- Conclusions 36

Chapter 2: Cell Culture 38
- Introduction 38
- Methods 40
  - Cell Culture 40
  - Cell Seeding 41
  - Live/-Dead assay 42
  - Cell morphology staining 43
  - MTT assay 43
- Results and Discussion 44
  - Live/-Dead Assay 45
  - Cell morphology staining 48
  - MTT assay 52
- Conclusions 57

Chapter 3: Future Directions 59

Supplemental Figures 60

Bibliography 66

List of Figures

Figure 1. Comparison of solution electrospinning and melt electrowriting. 11
Figure 2. Examples of MEW design and printing capacity. 13
Figure 3. Comparison of different hydrogel coated scaffolds. 19
Figure 4. Differences in pHEMA coating based on duration in solution. 20
Figure 5. Designs of scaffolds used in this thesis. 22
Figure 6. Graph of predicted shaker table speed in rpm based on speed setting. 25
Figure 7. Example image analysis using ImageJ. 26
Figure 8. Example box pore scaffold with and without pHEMA coating. 28
Figure 9. Coating densities of box scaffolds coated for the same duration at different agitation speeds. 29
Figure 10. Distinct morphologies observed with pHEMA coatings on box PCL scaffolds. 31
Figure 11. Proposed diagram of formation of mesh coatings. 34
Figure 12. Comparison of collagen to pHEMA coating. 36
Figure 13. Scaffold-drum suspension platform used in cell culture. 41
Figure 14. Results from Live/-Dead assay for non-coated and pHEMA coated scaffolds. 46
Figure 15. EthD-1 control experiments for pHEMA staining. 47
Figure 16. 24-hour cell morphology staining with DAPI and phalloidin 49
Figure 17. 48-hour cell morphology staining with DAPI and phalloidin. 50
Figure 18. 72-hour cell morphology staining with DAPI and phalloidin. 51
Figure 19. MTT assay results for scaffolds without cells. 53
Figure 20. MTT assay results for 48-hour cell seeding. 54
Figure 21. MTT assay results over course of three days. 56
Figure S1. MATLAB generated scaffold designs. 60
Figure S2. SEM image of pHEMA hydrogel made without PCL fibers. 61
Figure S3. High speed mesh coating. 62
Figure S4. Comparison of different dead stains of pHEMA coated scaffolds. 63
Figure S5. Channel breakdown of cell staining. 63
Figure S6. Stacked comparison of cell activity. 64
Figure S7. Stacked comparison of cell activity over three days. 65

List of Tables

Table 1. Agitation speed settings. 25
Table 2. Average fiber diameter and fiber spacing of MEW scaffolds. 27

Introduction: Scaffold-based Tissue Engineering

Tissue Engineering

Despite the medical advancements of the past decade, millions of individuals are left untreated due to disparities in organ supply and demand. Globally, this disparity in organ transplantation is recognized as a major public health challenge. Through transplantation of organs, it is possible to lower mortality rates and enhance the quality of life for people suffering from organ failure and an array of associated diseases. The true extent of this shortage is unknown, with many individuals never finding their way onto a transplant list (Giwa et al., 2017). This shortage is further exacerbated by poor matches, lack of infrastructure, limited transportation range, and overall expense (Dzobo et al., 2018). The field of tissue engineering (TE) was established to address this shortage by combining advances across disciplines to reduce the need for donor tissues by generating artificial replacement tissues and organs (Langer & Vacanti, 1993). This process relies primarily on the fields of medicine, engineering, and biology to understand, generate, and examine possible replica tissues. The field also examines methods of harnessing and elevating the body's natural healing processes with these replicas (Mao & Mooney, 2015). Many of the current limitations of organ transplant are addressed through the generation of synthetic replacement tissues and therapies, such as storage, transportation, and patient matching (Dzobo et al., 2018). Today, there is TE research on almost every tissue in the human body, each with its own unique formula working to replicate complex natural processes. These studies then work together to address this larger issue from multiple perspectives to progress towards a solution to this overall disparity.

The main strategy in TE is to mimic the natural tissue environment in order to promote cell growth and healing. This natural environment is termed the extracellular matrix (ECM), a noncellular support structure for the maintenance, replication, and repair of cells/ tissues (Lynch et al., 2021). To replace the ECM, the material used must provide the needed structural and mechanical support to the surrounding cells so that they maintain their intended function. The ECM also functions as a medium for the transmission of bioactive cues between cells and their environment, including cellular signaling, growth factors, environmental cues, and nutrients. This is accomplished by using porous materials to allow for the transportation of these cues. Finally, the ECM is vital to the natural repair of tissues because it can be broken down to provide a flexible environment for new growth. This can be achieved in a replica tissue through the use of biodegradable materials (Chan & Leong, 2008). These are all crucial considerations, because if the inserted artificial tissue does not match the native landscape, it is more likely to result in rejection, providing more harm than good (Lynch et al., 2021). The ECM is also not consistent throughout the body, so an understanding of the injury, cellular requirements, and composition of the specific area are instrumental to the intervention design. All of these components must, therefore, be balanced and achievable in the execution of a usable artificial tissue.

Due to its multidiscipline nature, TE draws inspiration from the fields of engineering, biology, material science, and medicine, resulting in a multitude of strategies to mimic the properties of tissues (Lynch et al., 2021). Key areas of focus for this project include the use of natural and synthetic materials, hydrogels, biological factors, cell constructs, and additive manufacturing. Material selection is essential in TE since the goal is to replicate the structural properties of the intended ECM. Natural materials, such as decellularized tissues, meet these requirements but are subject to high levels of variability and lack of control (Fonseca et al., 2020;

Mao & Mooney, 2015). The use of decellularized tissues also does not eliminate the need for native host tissues, perpetuating the reliance on donated tissue. Synthetic materials, on the other hand, are more tailored towards their application but require additional steps to ensure integration with host tissues (Fonseca et al., 2020). A key material in this conversation are hydrogels as they can fall in either category, are hydrophilic in natural, and are largely biocompatible (Lynch et al., 2021). Hydrogels have similar mechanical properties to soft tissues and the ECM but are often too weak to support themselves (Caliari & Burdick, 2016). 3D printed porous structures, termed scaffolds, have emerged alongside hydrogels to provide a structural support for cell attachment and growth of native tissues during injury repair (Chan & Leong, 2008). While materials alone can replicate the ECM, it is taken a step further when natural biological factors, such as growth factors or cellular products, are included as part of the design. These are typically incorporated through binding to the material or in a suspension and aim to promote cellular interactions (Caliari & Burdick, 2016; Dzobo et al., 2018). Cells can also be incorporated with the designed ECM in order to provide immediate support to the injury site (Neves et al., 2020). As these strategies are developed, they are then combined to create increasingly complex replica tissues.

An important cornerstone of the field of TE is additive manufacturing (AM), as the incorporation of scaffolds with this approach allows for more accurate replication of natural processes. AM, commonly referred to as 3D printing, is the process of creating a 3D object by layering material on top of itself based on a digital file. The most commonly used AM technique for TE is extrusion-based 3D printing due to ease of software accessibility and lower cost (Kumar & Sharma, 2021). This includes extrusion-based 3D bioprinting, which allows for printing with biocompatible hydrogels and factors, such as cells (Daly et al., 2021). The use of

3D printing for TE allows for scaffold personalization, as the digital file can be manipulated to meet the needs of a patient or specific application. (Paxton et al., 2020). The nature of the digital file also makes production readily reproducible, lending itself to high volume studies. Compared to previous methods of scaffold design, such as injection modeling, 3D printing allows for improved speed, reproducibility, and tailoring capabilities. Basic components of extrusion-based 3D printing include the material, which is processed into a liquid form, that is then forced through a nozzle via a pressure or feeding mechanism. If the material being used is melted, the printer head also contains heaters to maintain the needed temperature. The material is deposited onto a collector plate that can be heated or cooled based on the material requirements. Either the collector or nozzle is motorized in order to form complex structures in the X, Y, and Z planes (Kumar & Sharma, 2021). The creation of these 3D structures has allowed for a shift in the field from 2D studies to 3D studies of cell behaviors. This has allowed for deeper understanding of how cells interact with each other as well as their environment for further development of replica tissues (Fonseca et al., 2020). It has also highlighted the need to work on a size scale relevant for tissue structures, pushing the industry towards higher fabrication resolution, including smaller fiber diameter printing.

Melt Electrowriting

Melt electrowriting (MEW) is a high-resolution 3D printing technology designed to fill a gap in the need to generate complex, scaffolds with micro scale components. MEW serves as a middle ground of fiber diameter and control between extrusion-based 3D printing and another manufacturing technology termed solution electrospinning (SES). While extrusion-based 3D printing can generate precise scaffolds, it is limited by the size of the extruder with reported ranges of ~50-500 μm diameter fibers (Kade & Dalton, 2021). MEW is able to reduce this size

range by utilizing an applied electric field to stabilize a thin thread of molten filament, referred to as a jet, to produce 2-50 µm diameter fibers. This is inspired by a related technique, SES, which uses the electric field to stabilize a thin jet of filament that is then "whipped" to create submicron thin fibers. This whipping motion is caused by electrical instabilities between the jet and the collector plate and cannot be controlled, resulting in the formation of a nonuniform mesh rather than a scaffold. MEW prevents this phenomenon by maintaining a low flow rate, applied voltage difference, and a close range collector plate distance of 1-3 mm below the print nozzle. This is illustrated by Figure 1, which demonstrates the steps used to transition from MES to MEW, which was referred to as melt electrospinning writing at the time of this publication (Hochleitner et al., 2015).

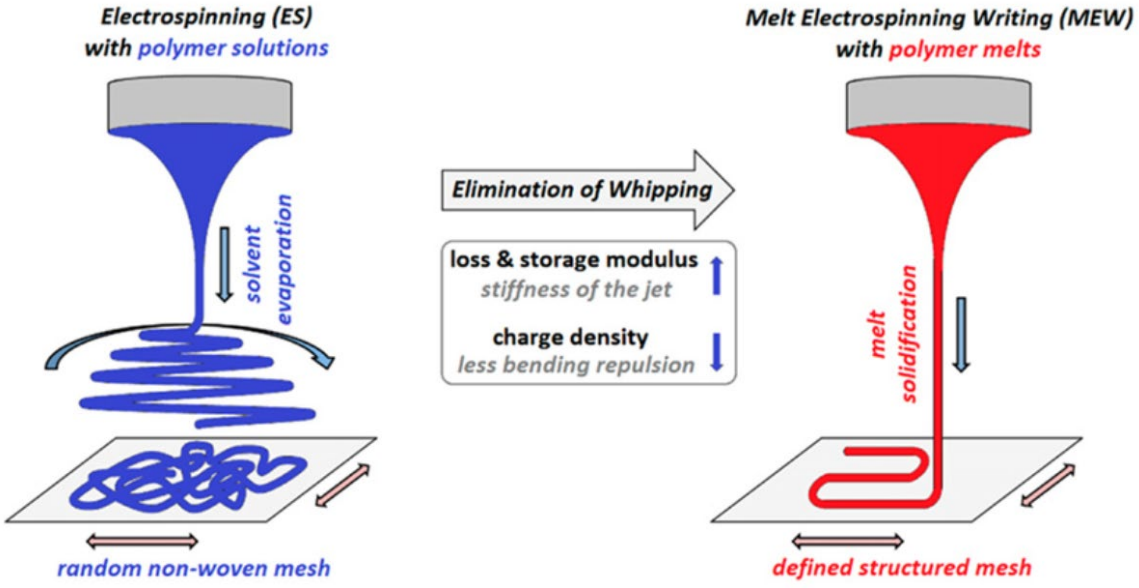

Figure 1. Comparison of solution electrospinning and melt electrowriting.

Schematic comparing the fabrication processes of SES to MEW and the transitions that allow for the formation of thin, controlled fibers (Hochleitner et al., 2015).

The jet and subsequently the fiber diameter can then be modulated by parameters that can be controlled throughout the printing process including the pressure, temperature, and material

extrusion rate (Kade & Dalton, 2021). The mobile collector plate then allows for the creation of highly specific structures by following a coded path, similar to other extrusion-based 3D printing processes. These thin, precise fibers thus make MEW an ideal candidate for the creation of porous scaffolds for TE.

MEW has emerged as a powerful platform for TE from both a material and design perspective. From a design perspective, MEW allows for the production of scaffolds with unique mechanical properties based on geometry and fiber pattern. Figure 2 demonstrates some of the complex design patterns research teams have achieved in order to test the mechanical and fabrication capabilities of this technology.

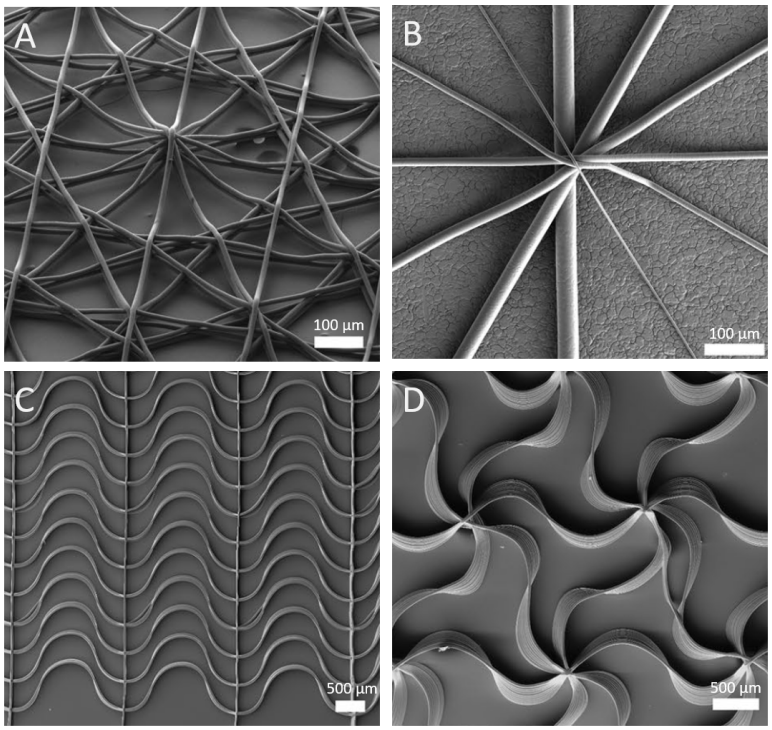

Figure 2. Examples of MEW design and printing capacity.

Through several studies, it has been demonstrated that MEW can be utilized to create complex designs with high accuracy during a single print. (A) dodecagon design (Youssef et al., 2019). (B) different fiber diameters in a single print ranging from 5-30 µm (Hrynevich et al., 2018). (C) sinusoidal design in a unilateral direction. (D) sinusoidal design in a hexagon design (Bas et al., 2017).

The micron thin fibers produced using MEW allow for the formulation of highly porous scaffolds, >90% vs 60-80% seen with other fabrication methods (Castilho et al., 2018). This is due to the two orders of magnitude difference between the printed fiber diameter and spacing between fibers. This porosity is ideal when working to replicate the ECM because it maximizes the amount of space for cells to grow and communicate, while still providing mechanical stability and attachment points (Chan & Leong, 2008). Because of the high porosity, MEW printed scaffolds are also ideal for reinforcing hydrogels in order to better mimic the mechanical properties of tissues (Visser et al., 2015). From a materials perspective, MEW is well-suited for translation towards *in vivo* applications because the gold-standard polymer used for printing is

medical-grade poly(ε-caprolactone) (PCL). PCL has a melting point of 60°C and rapidly solidifies, making it ideal for MEW printing. PCL is biocompatible, as well as biodegradable in the body over a period of several years. As a material, PCL also has a well-established track record of use in FDA-cleared medical devices, it is used in sutures, meshes, and some implanted devices (Kade & Dalton, 2021). This history is crucial for the relevance of these scaffolds for future clinical applications because it reduces the regulatory burden for demonstrating safety and efficacy of PCL for new medical interventions.

Project Motivations

Despite the promise of TE, there is still a lot of ground to cover before these processes can be used within the clinic. Overall, the initial focus in the field has been understanding the mechanical properties and dynamics of tissues, resulting in approaches that are too simple for successful application (Neves et al., 2020). By ignoring important cellular and environmental cues, many designs lack the ability to promote natural cell growth, key vascularization, and proper ECM production. In cell-based interventions, there are limitations in the acquisition of these cells as well as their maintenance (Dzobo et al., 2018; Mao & Mooney, 2015). It is preferable to acquire cells from the intended recipient of the therapy in order to mitigate immune responses, but these are limited in their ability to regenerate and grow *in vitro* (Dzobo et al., 2018). This process is complicated further in certain strategies because the cells then need to be seeded onto the scaffold, which is a time consuming and often unsuccessful process (Chan & Leong, 2008). From a materials standpoint, if research teams are developing novel materials that have not undergone rigorous testing compliant to regulatory standards, a significant quantity of *in vitro*, *in vivo*, and clinical testing is required. This process requires substantial funding, time, and effort which significantly delays any clinical translation. This, along with the developmental

work, means that these are still not cost-effective solutions. From a practicality side, these interventions have not reached a stage of timely or easily accessible production for implementation in clinics (Lynch et al., 2021). For these reasons, most of these studies are still in a proof-of-concept phase as research teams continue to expand upon both the available materials and the understanding of these complex biological processes.

The use of PCL means MEW is not immune to these challenges, as the synthetic polymer has been demonstrated to have poor cell adhesion properties. While PCL has a long history of clinical use, its hydrophobic nature proves problematic for cell culture due to poor adhesion, as noted throughout the field (Dash & Konkimalla, 2012; Kade & Dalton, 2021; Siddiqui et al., 2018). Cell seeding remains a very manual, low yield process, as many of the cells will fall through the pores and other will detach to preferentially grow on the culture-treated plastic of the well plate (Chan & Leong, 2008). This is further complicated by the challenges of visualizing successful cell attachments due to the disconnect between the 3D structure and microscope imaging of 2D planes. The combined challenges of seeding cells onto high porosity scaffolds manufactured from an inherently hydrophobic polymer has driven the development of several strategies to optimize scaffold surface properties to increase cell seeding efficiency. Numerous groups are working to address this issue through methods of hydrophilization, as summarized in a review by Kade and Dalton, including most commonly the application of sodium hydroxide (NaOH) (Bertlein et al., 2019; Kade & Dalton, 2021). Methods of improving these surface properties rely on altering the surface of the scaffold through means such as chemical modification, biological coatings, or embedding within a hydrogel. In order to maintain the clinical application of these scaffolds, this modification must be made of an approved material, limiting the possible choices.

Our Approach: Combination of Two Clinically Relevant Materials

One such clinically relevant coating is poly(2-hydroxyethyl methacrylate) (pHEMA), a porous hydrogel that has been investigated for applications such as wound repair, bone regeneration, and cancer treatments. The monomer, 2-hydroxyethyl methacrylate (HEMA) was first synthesized in the 1960s and used to create contact lenses (Zare et al., 2021). This was achieved when HEMA was polymerized in the presence of 40 wt% H_2O or less. When there is a higher concentration of monomer to water, a microporous hydrogel is formed that is not ideal for cell studies due to the limited diffusion of cellular signals and proteins through the hydrogel. When there is an even higher concentration of water to monomer (75 wt% H_2O and above), a macroporous hydrogel is formed that is ideal for cell culture due to its soft, spongy nature (Dalton et al., 2002). One drawback to pHEMA in vitro, however, is that it is a synthetic material, lacking essential biological cues for cellular growth that would be present in a natural material. Several studies have worked to address this limitation from multiple directions by functionalizing the pHEMA hydrogels with polypeptides, utilizing it as drug carrier, and conferring antibiotic properties (Paterson et al., 2013; Zare et al., 2021). While pHEMA has been studied for bioengineering applications on its own, few studies have examined it in a hybrid fabrication setting. This highly porous hydrogel is of interest for the coating of PCL fibers since it can benefit from the structural support provided by the scaffold.

This thesis will investigate the viability of pHEMA coated PCL scaffolds printed with MEW for cellular studies and development towards use in tissue engineering applications. Utilizing pHEMA to coat the PCL scaffolds is underpinned by a strong foundation of previous research on both materials in clinical settings, as well as efforts to improve each material individually for diverse applications. It is vital to understand how these materials interact with

each other, cells, and assay methods for *in vitro* testing prior to any possible clinical applications. While pHEMA has been assessed for cellular compatibility *in vitro*, these tests often revolve around the release of a compound into the media, rather than cellular growth on the surface of the hydrogel. To our knowledge, there are no studies examining the *in vitro* conditions of hybrid pHEMA, PCL scaffolds. This thesis will fill this gap in knowledge by leveraging three common cell culture assays in order to determine if these hybrid scaffolds are suitable for continued study in a TE context. The design of this construct lends itself to further optimization based on printing parameters, coating conditions, and hydrogel functionalization. This thesis provides a simple fabrication process with a multitude of applications, ideally suited for widespread development of TE solutions to increase synthetic tissue availability.

Chapter 1: pHEMA Hydrogel Coatings

Introduction

PHEMA stands out from other hydrogels because of the phase separation step during its polymerization in excess water. The polymerization process of HEMA has two distinct steps: phase separation, and gelation, which happen in a different order depending on the monomer to water ratio. When gelation occurs before phase separation, a stiff, microporous hydrogel is formed which is commonly used in the formation of contact lenses. When phase separation occurs first, the polymer is able to bead and form droplets, creating a macroporous hydrogel (Zare et al., 2021). This phase separation occurs because the polymer form, pHEMA, is not water soluble, unlike the monomer form, HEMA (Dalton & Shoichet, 2001). The phase separation also allows for the encapsulation of water molecules within the polymer droplets, resulting in a spongy, flexible material that resembles the ECM (Zare et al., 2021). Once attractive quality of these pHEMA hydrogels compared to other synthetic materials is its simple two-step polymerization process that allows for the formation of these macroporous structures. While other hydrogels rely on the inclusion of some pore-forming agent, pHEMA just requires an initiator and proper monomer-to-solvent ratio (Thakur & Thakur, 2018). As previously discussed, these macroporous structures are crucial in the field of TE for the purposes of cellular signaling and migration. The combined attributes of the ease of synthesis, macroporous nature, biocompatibility, and hydrophilic nature made pHEMA an ideal candidate for the coating of PCL scaffolds. Initial studies focused on whether the two materials were compatible without additional chemical modifications. The success of these first studies, demonstrated by lasting coatings on simple scaffolds, motivated further questions regarding how these coatings could be modified.

These pilot studies showed not only that these coatings were possible, but that they offered a unique morphology compared to previous methods. While other hydrogel coatings typically cling to the corners or fill the scaffold completely (Castilho et al., 2018; Löblein et al., 2021; Visser et al., 2015), the phase separated pHEMA coatings exhibited unique string-like structures that branch across the pores of the scaffold.

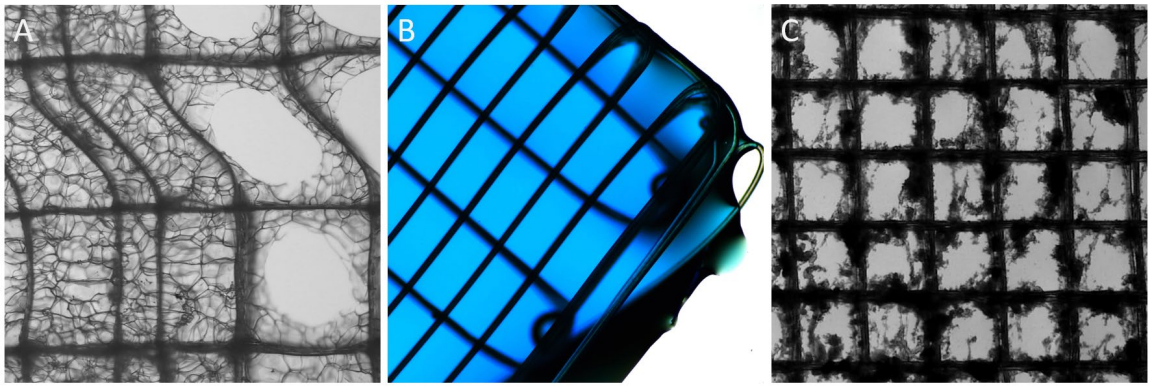

Figure 3. Comparison of different hydrogel coated scaffolds.

Three different hydrogel coatings on MEW PCL scaffolds with differing morphologies. (A) silk coating demonstrates both filling of pores as well as clinging to the corners (original work, unpublished). (B) hyaluronic acid hydrogel coating, colored blue with food coloring, demonstrates uniform filling of pores. Image from Alycia Galindo, unpublished. (C) pHEMA coating demonstrates webbing morphology (original work, unpublished).

There was also the formation of bead-like structures along both the PCL fibers, similar to water drops on a spider web. These interesting findings prompted questions on how else these coatings could be altered. In order to study the dynamics of these pHEMA coatings, parameters such as agitation, duration, and differing reactant concentrations were investigated. These were chosen because of the long duration of phase separation during the polymerization process, providing a possible method for experimental coatings. Initial pilot studies demonstrated the relevance of when the scaffold was placed in the solution compared to the onset of phase separation, as well as the duration the scaffold spent in the solution as shown in Figure 4.

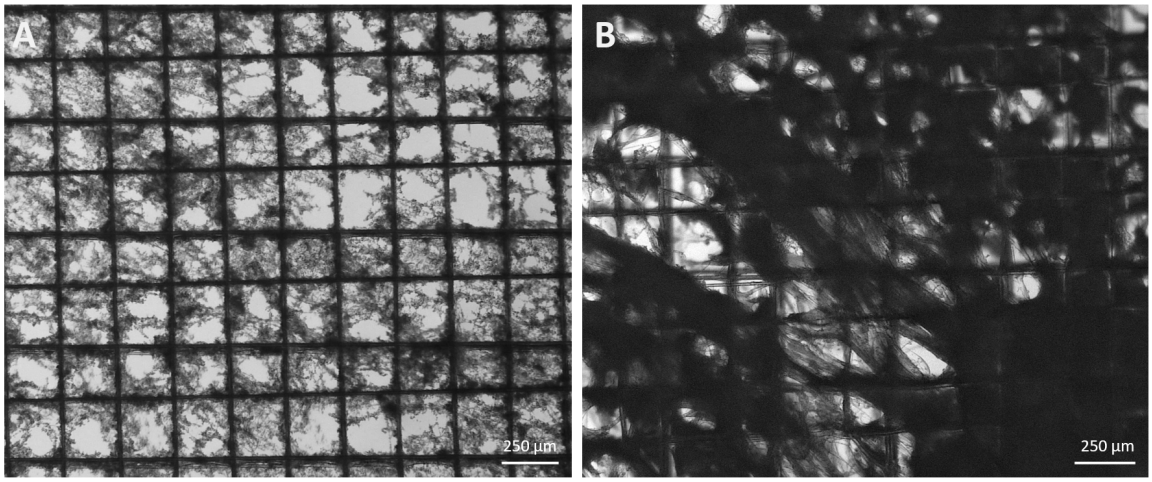

Figure 4. Differences in pHEMA coating based on duration in solution.

PCL scaffolds were coated in pHEMA solutions 30s post phase separation on the benchtop, (A) scaffold in solution for 40s (B) scaffold in solution for 1:40s. Images taken with a light microscope, scale bar 250 µm.

This indicated that each solution could only be used once in order to achieve similar coatings, and that specific timing conditions would be needed to investigate other coating parameters. Agitation was a point of interest due to the fact that pHEMA is denser than water. It was shown in a previous study that this phase separated pHEMA could be separated from the water at a high enough centrifugal force to create porous tube structures. These tubes exhibited differing morphologies at higher vs lower speeds, demonstrating a correlation between hydrogel morphology and agitation (Dalton & Shoichet, 2001). While these studies were conducted at significantly higher speeds than those needed to coat scaffolds, it showed a possible avenue for altering the coatings. Thus, the first focus of this thesis aimed to investigate if different coating morphologies were possible based on altered agitation speeds.

Methods

Scaffold Design and Fabrication

In order to fabricate MEW scaffolds, a computer must be able to communicate to the printer when and where to move. This line of communication is G-code, a coordinate-based programming language that directs the positioning of the MEW axes to move the collector in programmed directions to fabricate high precision scaffold designs. Scaffolds used for this study were generated using a custom MATLAB code generated by Dr. Ievgenii Liashenko (Figure S1). This code is used to develop the shape, spacing, and layer number for the scaffolds. This MATLAB code then outputs the design as G-code, which is compatible with the printer. There were two types of scaffolds used in this study:

1. Box pores to visualize the stringing and coating effect
2. Triangle pores to investigate the coating on a more application-relevant scaffold

Scaffolds were fabricated using a custom-built MEW printer designed by Dr. Ievgenii Liashenko. The two scaffold designs were printed based on the parallel fiber lines spaced at 250 μm, and on either the 0/90 degree fiber angles (box pores), or 0/72/144/216/288 degree fiber angles (triangular pores). These degrees represent the rotation in the orientation that the fibers were placed. Both scaffold designs were printed into circles of 14 mm diameter to fit into the well plate with 16 mm diameter. Both designs had an equal number of fiber layers set to 20, either 10 fiber layers by 2 angles for the box pore scaffold, or 4 fiber layers by the 5 angles for the triangle pore scaffold. No turning loops were used at the scaffold edges, while 0.5s pauses were introduced after the long linear moves to compensate for the jet lag to achieve defined scaffold edges and preserve constant fiber spacing. Medical-grade PCL (PC12, Corbion) was heated to 75°C and ejected from the 25G nozzle, protruding 1 mm from the printhead, and set at

3mm gap from the glass slide resting on a metal substrate. Printing pressure was set to 2.0 bar, and 4.8 kV voltage was applied to the collector. The translation speed was set to 500mm/min.

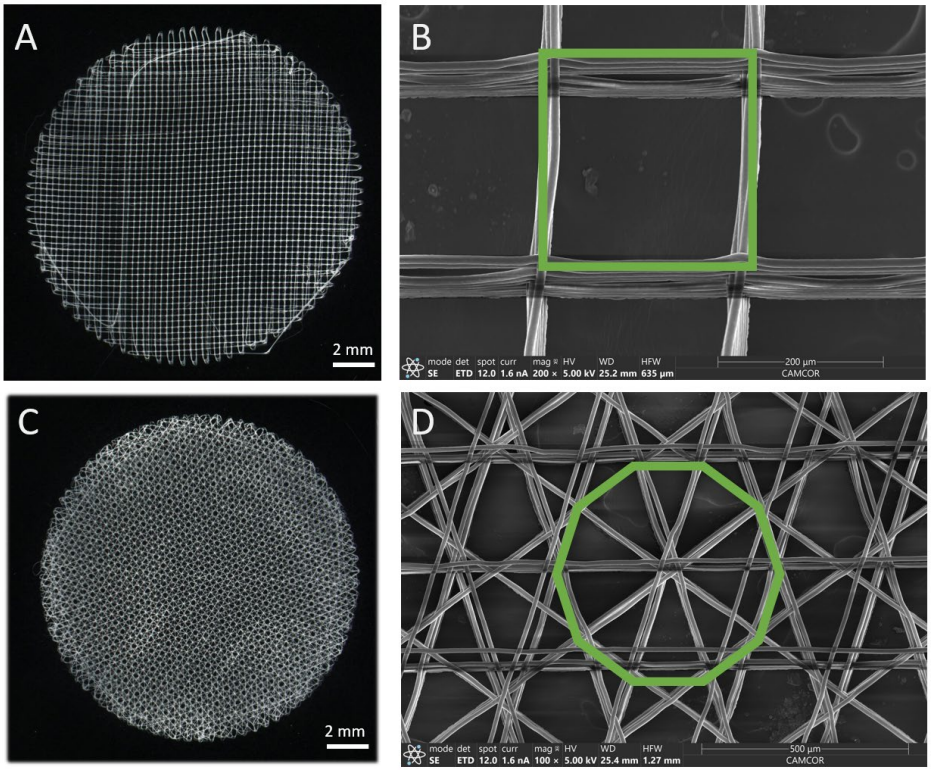

Figure 5. Designs of scaffolds used in this thesis.

Box pore scaffold design taken with (A) Keyence microscope (B) Scanning electron microscope (SEM) Triangle pore scaffold design taken with (C) Keyence microscope (D) SEM. Scale bars 2mm (A,C) 200 µm (B) and 500 µm (D).

Box pore scaffolds were chosen as they are common within the field due to the simplicity of the G-code (Kade & Dalton, 2021). The large, uniform pores created proved to be ideal for visualizing the pHEMA coating and were used for the majority of the coating analysis. The triangle pore scaffolds were added for the purpose of cell culture analysis to assess a more complex scaffold design. These scaffolds were designed with similar fiber diameter, spacing, and layers to isolate the change in fiber placement between samples. Scaffolds were measured using a Keyence microscope to confirm their dimensions.

NaOH Pretreatment

As a baseline treatment, all scaffolds were sterilized with 70 % ethanol and chemically pretreated with NaOH. The NaOH pretreatment physically etches the fiber surface, reducing the hydrophobicity of PCL. This is key when designing components for TE, since more hydrophobic materials have lower rates of cell adhesion and recognition (Bertlein et al., 2019; Niemczyk-Soczynska et al., 2020). The method used in this study was based on methods from three sources (Abbasi et al., 2020; Bosworth et al., 2019; Zhou et al., 2020). Scaffolds were left in 1 M NaOH for one hour and rinsed three times with dH_2O, then left to sit in dH_2O overnight before use.

PHEMA coatings

PHEMA hydrogels were synthesized fresh each day for scaffold coating based on procedures developed by the Dalton lab (Dalton et al., 2002; Dalton & Shoichet, 2001). 99% HEMA was purchased from Sigma Aldrich. The pHEMA hydrogels were formed using a redox initiator combination of 10% Ammonium Persulfate (APS) and 99% Tetramethylethylenediamine (TEMED). An 80:20, dH_2O:HEMA mixture was made and allowed to sit until homogenous. This concentration was chosen since it results in phase separation before polymerization, creating a porous, spongy hydrogel (Dalton & Shoichet, 2001). Once homogenous, 2 wt% by monomer APS was added to the solution. Once this solution was again homogenous, 0.2 wt% by monomer TEMED was added. The reaction was allowed to sit undisturbed while waiting for phase separation to begin, noted when the solution began to turn opaque. A scaffold was placed in the solution 30 s post phase separation and allowed to sit on the bench top for 80 s. These conditions varied slightly based on the timing or agitation being investigated. At time, the scaffold was retrieved from the solution and placed in dH_2O to remove any excess HEMA and left overnight. This process was optimized for this thesis so that the phase

separation would occur at ~5 minutes, as well as ensure that the scaffold was not overly coated so that the pores and geometries were still expressed. This is important for future applications since scaffolds are designed with specific parameters based on its intended application, so the pHEMA coating has to be thin enough to not obscure these features.

Agitated pHEMA coatings

Agitation was introduced to the coating process using a Barnstead Thermolyne Type 50800 Rotomix shaker table to agitate the HEMA: water solution when the coating the scaffold. This method provided a consistent source of movement during the selected coating duration. The shaker table with designed with a dial of increments from 0 to 10 to represent different speeds. These speeds settings were converted to rotations per minute (rpm) by counting the number of complete rotations in one minute for each speed setting possible, 1-3. These values were then graphed and fitted with a line of best fit in order to approximate the remaining speed settings, as shown in Figure 6. The resulting rpm values for each speed setting are shown in Table 1.

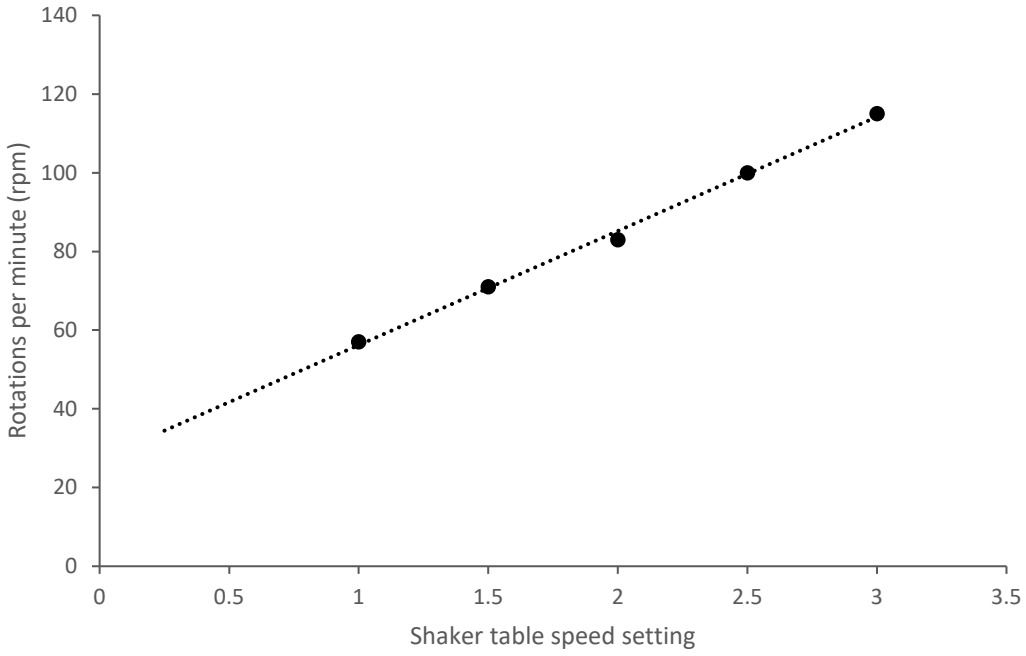

Figure 6. Graph of predicted shaker table speed in rpm based on speed setting.

RPM for specific speed settings was determined by counting the rotations completed in a minute for each setting possible. These were plotted and fitted with a line of best fit with the equation $y = 29x + 27.2$

Speed Setting	rpm value based on graph
1	56.2
2	85.2
3	114.2
4	143.2
5	172.2
6	201.2
7	230.2
8	259.2

Table 1. Agitation speed settings.

The corresponding rpm values for each dial setting of the shaker table were calculated based on the line of best fit.

Image analysis

pHEMA coatings were analyzed using ImageJ, an open-source application used across many scientific disciplines for image analysis. Scaffolds were imaged after coating with an Olympus SZX12 light microscope while the pHEMA was still hydrated. These images were then cropped in ImageJ to 700x700 pixels, visualizing exactly 9 pores including bounding fibers, in order to ensure an equal number of fibers present in each image. This was repeated across the image eight times while maintaining equal pore counts. Images were converted to gray scale, and the threshold was adjusted so that only the pHEMA and scaffold fibers appeared as black pixels, as shown in Figure 7, with the background as white pixels.

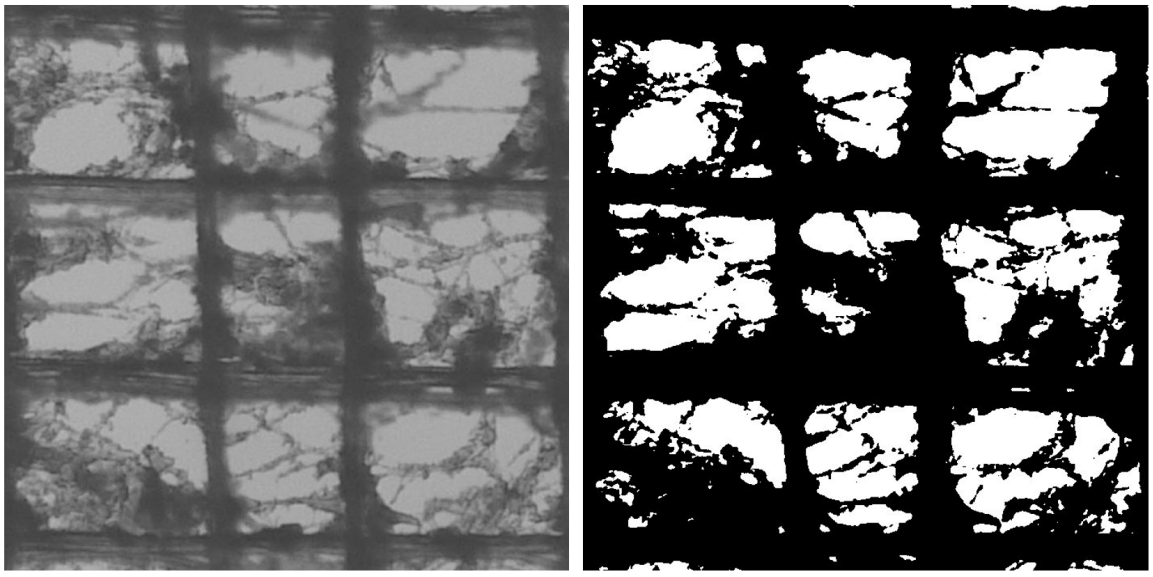

Figure 7. Example image analysis using ImageJ.

Images were cropped from the main image to a 700x700 pixel box and then adjusted so that only the scaffold and pHEMA coating were selected for with black pixels.

The number of black and white pixels was counted, allowing for a calculation of the percent of the image occupied by the scaffold and coating. These values were averaged for each scaffold (n-X), then averaged for each speed for an overall black pixel percentage (N-X). From this value, the percentage of black pixels in a non-coated scaffold was subtracted to yield the coating

percentage. Results were reported as average ± standard deviation and a student's t-test was performed to assess the statistical significance between groups, where $p<0.05$ was considered significant.

Scanning Electron Microscopy

Scaffolds coated with pHEMA were prepared for Scanning Electron Microscopy (SEM) using both a freeze-drying process and air-drying. For freeze-drying, coated scaffolds were hung on binder clips and suspended on a 3D printed rig before being placed in the freezer at -20 °C. After several hours, the scaffolds were dried using a vacuum pump lyophilizer. Samples that were air-dried were allowed to dry out in their plastic storage case. Two different techniques were used to prepare and image samples. The first set of samples was imaged on the SEM under low vacuum detector (LVD) and resulted in lower resolution images than desired. The second set of samples was coated with 5 nm of platinum before imaging using a sputter coater. Platinum sputter coating allowed for the use of the Everhart–Thornley detector (ETD) of the SEM. ETD is a secondary electron and back-scattered electron detector which has increased resolution compared to the LVD.

Results and Discussion

In order to confirm that the parameters of the scaffolds match the print pattern, the scaffolds were imaged and measured using a Keyence microscope, shown in Table 2.

Scaffold type	Fiber diameter (μm)	Fiber spacing (μm)
Box pore	11.6 ± 0.28	208.3 ± 8.14
Triangle pore	11.3 ± 0.68	221.67 ± 8.02

Table 2. Average fiber diameter and fiber spacing of MEW scaffolds.

The following table shows the average fiber diameter and fiber placement for both MEW scaffold types used. (n=3)

These results demonstrate that while the scaffolds do not follow the expected fiber spacing of 250 μm, they remain similar to each other. While these discrepancies do not interfere with the findings of this study, they are important for any follow-up studies to ensure scaffolds follow the printed dimensions rather than the programed dimensions.

The first important finding of this study was that the pHEMA hydrogel adhered to the PCL scaffolds, providing a method for adapting these scaffolds for improved biological application. These coatings spread across the pores of the scaffold, creating an organic structure along multiple layers, as shown in Figure 8.

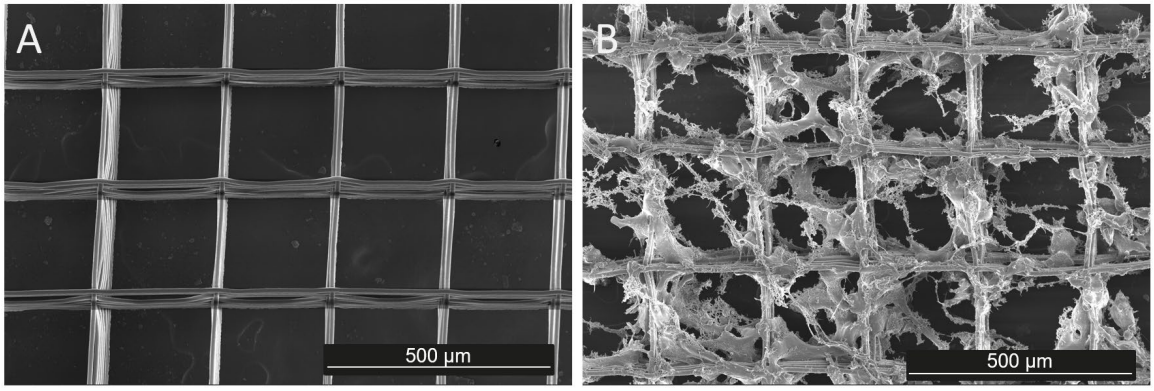

Figure 8. Example box pore scaffold with and without pHEMA coating.

(A) Plain box pore scaffold without any pHEMA coating. (B) Box pore scaffold with pHEMA coating, coated for 80 s at a speed of 172 rpm. Both samples were platinum coated and imaged with SEM, scale bar 500 μm.

These organic coatings inspired the subsequent investigation of how these coatings could be modulated by altering timing, duration, and agitation. The goal of these investigations was to determine if there were any trends in the coatings that could be controlled in order to generate reproducible scaffolds with tunable characteristics. To first assess the role of agitation in the coating process, scaffolds were coated for 80 s to ensure coating uniformity. This time was selected because it resulted in high levels of coverage while preserving most of the original scaffold morphology for non-agitated scaffolds, as shown in Figure 9A. The intended

morphology of a scaffold is key in TE, since it is designed to replicate the native tissue structure. Therefore, it is important to select a coating mechanism that maintains these structures as much as possible. Through comparison of the different timing parameters, the coating density was observed to decrease with increased agitation speed. These findings are reinforced by the image analysis, which demonstrates an overall decrease in coating density through the percentage of black pixels in each image, as shown in Figure 9.

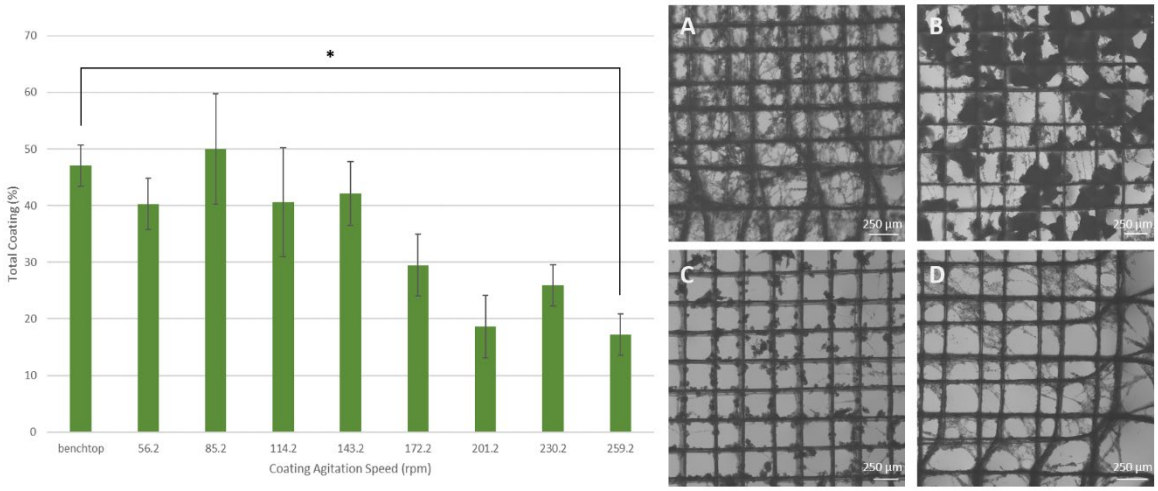

Figure 9. Coating densities of box scaffolds coated for the same duration at different agitation speeds.

The graph on the left shows the coating density at each agitation speed, reported as average ± SD (n=16). The images on the right are representative of four coating speeds. Each scaffold was coated for 80 s and then placed in a water bath before imaging with a light microscope. (A) benchtop (B) 114 rpm (C) 172 rpm (D) 230 rpm. Scale bars of 250 µm. * $p < 0.05$.

It was found that the coatings decreased from 47 ± 3.63% to 17 ± 3.65% at agitation speeds of benchtop to 259 rpm respectively ($n=16$, $p < 0.05$). This significant decrease in coating density demonstrates an ability to modulate the available scaffold space based on the speed at which the scaffold was coated. For TE, scaffolds are ideally designed to mimic a specific architecture, suggesting higher agitation speeds are favorable since they compromise less of the intended porosity. Lower agitation speeds are still valuable coating methods in settings where scaffolds

are designed with excessively large pores or shorter coating durations are used. It is important to note with the image analysis results that some percentages are overrepresented due to poor fiber alignment, inflating the coating percentage compared to the non-coated fibers. This is due to the increased visibility of improperly aligned black fibers in some samples. Overall, these findings demonstrated a clear trend in the influence of timing and agitation on the coating density, as well as trends in coating morphology.

Through these experiments, several distinct morphologies were observed: clumps, small spheres, mesh, and strings. These different coating morphologies do not seem to be correlated with a specific coating style, but rather a consequence of a range of parameters. These different coating morphologies are shown in Figure 10, where each scaffold underwent a slightly different coating procedure related to speed, timing, and initiator concentrations.

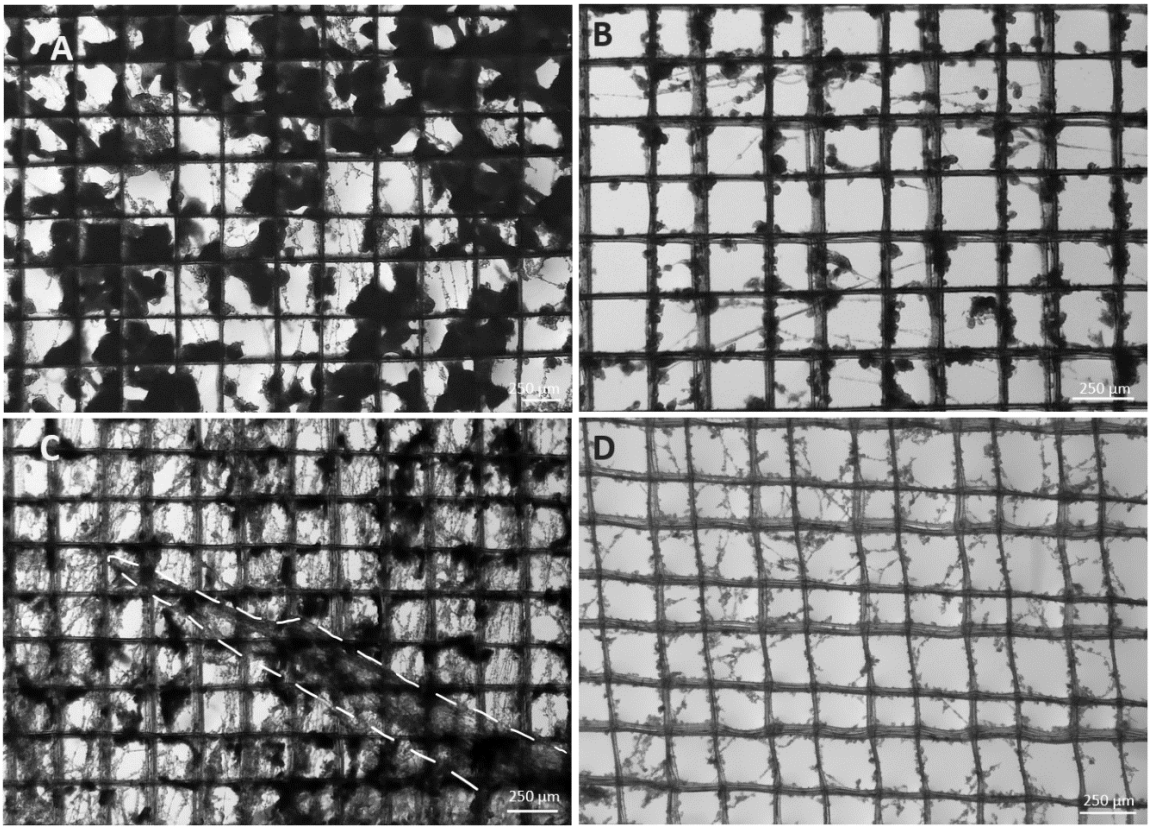

Figure 10. Distinct morphologies observed with pHEMA coatings on box PCL scaffolds.

Different patterns in the coatings became apparent across the different coating styles. (A) clumping of pHEMA. (B) small spheres of pHEMA forming on the scaffold fibers. (C) mesh coating along the back of the scaffold, with a folding and condensing of this mesh in the foreground, outlined. (D) small strings of pHEMA that are contained within one or a few pores as well as small spheres. Images taken with a light microscope, scale bar of 250 µm.

Figure 10A demonstrates the large clumping formations that are seen across a large subset of coating conditions, including lower agitations speeds, high initiator concentrations, and long coating durations. The clumps typically favor the corners of the scaffold, likely due to the increased binding area or ease of accumulation. It is hypothesized that the low speeds of agitation allow for the formation of large clumps of hydrogel within the solution that then become trapped within the pores of the scaffold. This trend is consistent with observations made regarding cell attachment, which also favor the corners of scaffolds due to intersecting fibers providing increased support for attachment and growth (Han et al., 2021). For these reasons, it is

suspected that these large clumps would not be favorable for cell seeding experiments, since these dense clumps of pHEMA are utilizing the spaces desired by cells and lowering the porosity of the scaffolds. While the pHEMA hydrogel is porous and can allow the diffusion of biological products, it is hypothesized that such a dense formation as seen in these clumps would not be conducive, as it would isolate cell populations that form on top of the clumps. For these reasons, these coating styles should be avoided for any possible cell culture work. These coatings do offer an advantage in settings where filling of pores is desired, such as the creation of a specific network. While a more predictable and common coating style, these large clumps serve as boundary conditions for establishing reliable coating parameters for TE experiments.

Similar to the large clumps, Figure 10B shows the small spheres of pHEMA that form along the PCL fibers. These small spheres typically form at higher agitations speeds or lower initiator concentration with a range of sizes. Spheres are observed on their own, forming along the PCL fibers as well as in conjunction with other coating morphologies, such as within the mesh or stings of pHEMA. These spheres are similar to the spheres observed in SEM images of pHEMA hydrogels formed by the phase separation process that gives pHEMA its distinct spongy, porous structure (Figure S2). One possible explanation for the formation of these spheres at medium-to-high agitation speeds is that the addition of agitation forces disperses the pHEMA within the solution, preventing the formation of large polymer networks. Instead, as the small polymer droplets formed, they collide with the PCL fibers and form around the scaffold, forming the beaded fibers. These droplets can then grow as they collide with more pHEMA in solution or stretch due to the agitation forces. Further exploration of the timing condition with the formation of the small spheres versus the large clumps of pHEMA solution could allow for a deeper understanding of the different parameters controlling these two coating styles. These

small spheres could be beneficial in TE conditions by serving as a point of attachment for cells or providing a roadblock to cell growth. Both conditions would depend on how the pHEMA is functionalized based on the cell type used. Overall, these small spheres align with other observed pHEMA structures and exist a narrow range of coating conditions, demonstrating the scope of possibilities for these coatings.

The distinction between the other coating morphologies observed, mesh and string, is more nuanced, and likely will require further studies to establish if they are distinct trends. From the experiments conducted, the mesh coatings are denser, spread across several pores, and appear more interconnected. These mesh coatings also typically appear along one plane of the scaffold, demonstrating that the network may have already formed in solution prior to the addition of the PCL scaffold. This suggests a possible plastering mechanism similar to hydro dipping, where the scaffold becomes coated when entering or leaving the pHEMA solution based on the position of these preexisting meshes. Since pHEMA is rapidly undergoing polymerization once the phase separation begins, there are likely several networks forming within the solution at a given time. As the scaffold comes in contact with these networks, it becomes stuck to the scaffold, likely due to the hydrophobic methacrylate group. Once attached, the mesh can continue to grow based on reacting monomer units within the solution, or connect with another mesh, resulting in many interconnecting polymer fibers, as proposed in Figure 11.

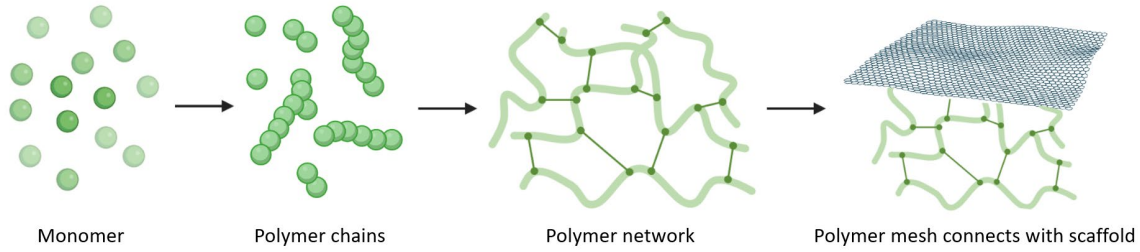

Figure 11. Proposed diagram of formation of mesh coatings.

A proposed mechanism for the formation of these mesh coatings is that, as the polymer networks form, they come in contact with the scaffold entering the solution. This results in the formation of a mesh structure along the scaffold.

Insights can be gained from studying these styles of coatings, due to the differences in appearance depending on the coating conditions. For scaffolds coated on the benchtop, these mesh coatings exhibited a wide variety of directionalities along multiple layers of a scaffold. This could support the idea of multiple points of contact between the scaffold and pHEMA; when the scaffold was dropped in solution, while it sat in solution, and when it was retrieved from solution. All of these processes would cause different interactions with the forming hydrogel networks, explaining the variety in hydrogel alignment relative to the PCL fibers. This is demonstrated in Figure 10C, where multiple directions of pHEMA mesh are demonstrated, as well as an area where the mesh has clumped together, outlined in white. While this clumping could be due to a higher concentration of coating in that specific area, it could also indicate a space where the mesh was disrupted, possibly due to the scaffold being removed from the solution. This also explains why at some of the higher agitation speeds, there were areas of dense coating coupled with areas of little to no coating on the same scaffold (Figure S3). If, during the agitation process, the scaffold was to come in contact with one of these preformed hydrogel networks, it would result in an area of high coverage with directional fibers from the collision.

Overall, a greater understanding of these mesh coatings would provide insight for both the formation of the pHEMA hydrogels as well as how pHEMA interacts with PCL.

The final coating morphology observed consists of small pHEMA strings that are often accompanied by the small spheres described earlier. These fine strings differ from the mesh coating because they are contained within one pore or a small cluster of pores within the scaffold. They are less uniform than the mesh fibers, and instead spread within the pore in a variety of patterns resembling natural structures like coral. These strings appear to be less strained than those in the mesh coating and are fewer in number and density throughout the scaffold. These strings arise due to a more limited opportunity for coating the scaffold, explaining their low concentration. This aligns with the fact these strings are observed at low initiator concentrations, short coating durations, and medium-to-high agitation speeds. For these reasons, these structures have not been observed in many samples due to testing abilities. Another key observation is that these string form in conjunction with the sphere structures discussed before. It is possible that these strings form due to the stretching of the spheres with the addition of agitation or low initiator concentrations, allowing for prolonged polymerization rates. These spheres could also cluster together along these strings, allowing for the formation of structures similar to the mesh at a smaller scale. While the least can be said about the conditions favoring the formation of these small strings, they could provide a favorable structure of cellular attachment in situations where the mesh coatings are too dense. This provides many avenues for scaffold functionalization based on the understanding of optimal cell culture conditions as well as native tissue structures.

Conclusions

These studies demonstrate the complex morphologies of pHEMA coated PCL scaffolds while using a simple phase separation and submersion technique. By altering parameters such as coating duration, agitation, and reactant concentrations, a variety of coating morphologies can be created using this two-step reaction mechanism. This demonstrates a simple, cost-effective, and time effective method for altering the geometry of PCL scaffolds with organic structures that cannot be achieved with MEW. These organic structures could be beneficial in TE contexts due to the increased surface area of the scaffold while maintaining high levels of porosity. The relevance of these pHEMA structures is demonstrated in Figure 12 when comparing the freeze-dried pHEMA coating to freeze-dried collagen, one of the most prominent structural components in the body (Caliari & Burdick, 2016).

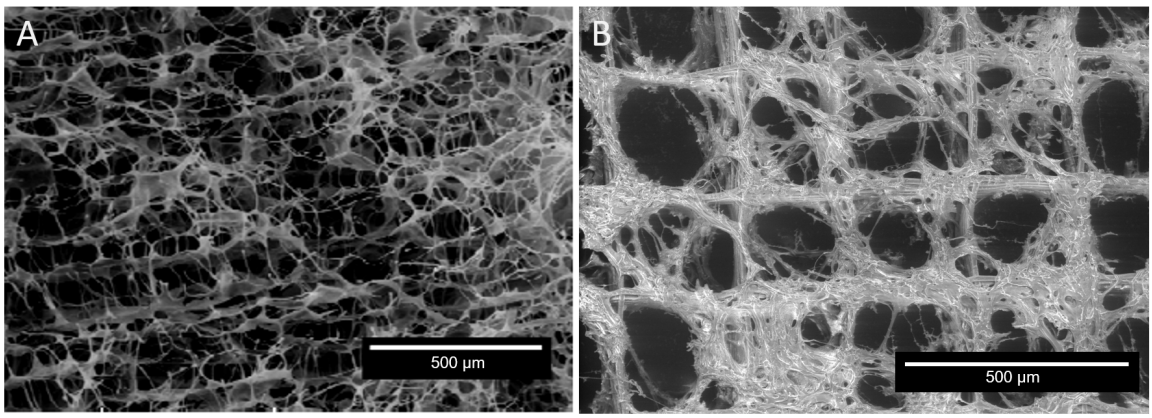

Figure 12. Comparison of collagen to pHEMA coating.

pHEMA coatings provide interesting applications for TE due to their similarity in structure to common ECM factors, such as collagen. (A) SEM image of freeze-dried collagen (Vranceanu et al., 2012). (B) Low vacuum SEM image of pHEMA coated box pore scaffold, coated on benchtop. Scale bars 500 µm.

Since one of the primary objectives of TE is to replicate the natural cellular environment, pHEMA provides a step in this direction with a simple, reproducible procedure. These organic structures, while beneficial, do pose a challenge as they are not readily predicable, resulting in

levels of variation between each scaffold. Through a greater number of studies, more concrete trends could be established to aid in this process, making the coatings more streamlined for TE applications. Despite these limitations, these pHEMA coated scaffolds provide a valuable combination of two clinically relevant materials for progress towards advances ECM replicas.

Chapter 2: Cell Culture

Introduction

In order for these pHEMA coated scaffolds to be applicable in a clinical setting, they must first be demonstrated to work *in vitro*. *In vitro* studies, studies conducted outside of a living organism, are vital to the research process as they are low cost, high output methods of assessing the relevance of an intervention based on cellular interactions. If these studies prove successful, they can then be translated into *in vivo* studies, studies conducted in a model organism, to gain a better understanding of how the intervention interacts within a complete organism, rather than an isolated cell type (Sobacchi et al., 2018). The results of these *in vitro* studies are assessed by determining cell characteristics, such as cell products produced, morphology, and viability. These tests rely on the use of different chemical assays or stains, which could have adverse effects on untested materials (Gao et al., 2022; Zhou et al., 2020). Despite the use of both PCL and pHEMA in clinical studies, very few studies have used the two materials together in a cell culture setting, resulting in few references for staining and assay results. For the purposes of this thesis, three assays were selected due to their prevalence in the literature as well as the diversity of reaction mechanisms to provide a comprehensive review. This will allow for the establishment of relevant baselines within the lab, enabling future complex studies of these materials in a cell culture context.

Three main assays were selected to establish a toolbox of compatible assessments for pHEMA coated scaffolds. The assays selected were a Live/-Dead assay, cell morphology staining, and an MTT assay based on their use throughout other labs, range of relevant information, and applicability to future studies in the lab. A Live/-Dead assay was selected based on its simple readout for cell viability. This method utilizes two fluorescent dyes that rely on cell

membrane integrity in order to produce a fluorescent response. The first dye, Calcein AM, fluoresces green in live cells based on transportation through the cell membrane, where it interacts with esterase within the cell, converting it to calcein. This conversion allows for green fluorescence and subsequently traps the converted molecule within the cell, preventing random fluorescence throughout the sample. To stain the dead cells, ethidium homodimer-1 (EthD-1) enters cells with compromised membranes, indicating cell death, and binds exposed DNA. As EthD-1 binds DNA, it becomes strongly fluorescent, allowing for the identification of dead cells. Overall, this assay provides a method of assessing if this pHEMA coating results in cytotoxicity, as well as if the pHEMA or PCL reacts with either chemical to produce a fluorescent response.

Cell morphology staining was assessed due to its relevance for understanding cell behavior. One of the key-focuses when shifting to a 3D model for cell studies is examining the differences in cellular behavior compared to a 2D study. The hope is that by using a 3D culture, cells will exhibit morphologies similar to those seen in host tissues, allowing for more accurate assessments of cell behavior (Fonseca et al., 2020). The two stains used for this study were 4′,6-diamidino-2-phenylindole (DAPI) and Phalloidin. DAPI is used to stain the cell's nucleus since it enters the excited state when bound to DNA, resulting in a blue fluorescence that can be detected using fluorescent microscopy. Phalloidin is used to bind actin, one of the main components of the cytoskeleton, in order to determine the cell morphology at the time of fixation. Phalloidin itself is not fluorescent, so it is labeled with a fluorophore in order to produce a fluorescent signal, typically red or green, when bound to actin. Together, these stains allow for the assessment of important structural characteristics.

An MTT assay was selected since it demonstrates cellular activity beyond alive or dead. MTT assays are used in cell culture to determine the metabolic activity of the cells based on

colorimetric analysis. MTT (3-(4,5-dimethylthiazolyl-2)-2, 5-diphenyltetrazoliumbromide) is a tetrazolium salt that is yellow until reduced by NAD(P)H dependent enzymes found in cells, resulting in the production of purple formazan crystals that are water insoluble. NAD(P)H is only present in high concentrations in cells actively using metabolic pathways, which allow for the breakdown of glucose, a simple sugar, to key components for cellular function, energy, maintenance, and division (Ghasemi et al., 2021). This means that these crystals represent cells that are not only alive, but actively growing and dividing. These crystals can then be dissolved with isopropyl alcohol (IPA) to create a solution that can be quantified using colorimetric analysis. The intensity of this purple corresponds to the overall metabolic activity of the cells and is measured on a scale of relative absorbance. A dark solution will read with a high relative absorbance due to the lack of light penetrating the solution, indicating high levels of cellular activity. While the principles of these assays are understood, it is important to screen them prior to *in vitro* analysis to understand any false positive results that may occur due to the hybrid scaffold.

Methods

Cell Culture

The cell line used for these experiments was NIH-3T3 labeled with green fluorescent protein (GFP), a fibroblast cell line that is genetically altered to express GFP. These were selected due to the robustness of fibroblasts for initial cell adhesion studies, as well as the GFP marker allowed for location and analysis of cell morphology without staining the samples. Cells were cultured at 37 °C at 5% CO2 in a sterile Heracell VIOS CO2 Incubator (Thermo Scientific) and passaged every 2-3 days to prevent full confluency. Sterile techniques were used when working with any cell samples using a Labconco logic plus biosafety cabinet.

Cell Seeding

All scaffolds were prepared under sterile conditions and soaked in cell culture media prior to cell seeding. All scaffolds were left in 0.1 M NaOH for 30 minutes then rinsed with PBS three times. This procedure was altered to align with other cell culture experiments performed within the lab. Only benchtop pHEMA coatings were used for these experiments due to complications in introducing the agitation while maintaining sterile conditions. Scaffolds were placed on an elevated platform, similar to a drum shown in

Figure 13, so that when the cells were added, they are not in direct contact with the well plate to promote adhesion to the scaffold.

Figure 13. Scaffold-drum suspension platform used in cell culture.

This scaffold-drum system was designed to elevate scaffolds above the bottom of cell culture well plate to promote cell attachment. The scaffold would be placed on top of the left half and then secured in place with the right half, as shown in the bottom images.

Scaffold-drum assemblies were placed in the center of the wells of a sterile, non-treated, 24-well plate. The scaffolds were seeded with 20,000 cells each in 20 μL of culture media in a droplet placed in the center of the scaffold. This allowed for a high level of cell spreading across the scaffold while also ensuring there was not too much media present, causing cells to wash away.

Scaffolds were then incubated for 3 hours at 37 °C. After, the scaffolds were removed from their elevated platform and placed in the bottom of a new well. 1 mL of media was added on top to ensure the cells did not dry out. Cells were allowed to grow for 24, 48, or 72 hours before analysis.

Live/-Dead assay

A Live/-Dead assay was conducted using EthD-1 and calcein AM from ThermoFisher. From the 2 mM stock solution of EthD-1, a 4 μM working solution was created by dilution with sterile PBS. From the 4 mM stock solution of calcein AM, a 2 μM working solution was created by adding the calcein AM to the same EthD-1 solution. The scaffolds were moved to a well containing PBS for a wash step and the PBS was aspirated. 200 μL of this working solution of EthD-1 and calcein AM was added to each well and incubated for 30 minutes. These concentrations and incubation times were selected based on previous studies and recommendations from ThermoFisher. Images were taken on an Echo Revolve microscope at a wavelength of 485 nm to view the calcein AM stained cells and 530 nm to view the EthD-1-stained cells.

Cell fixation

Prior to any histology, such as cell morphology staining, samples must be fixed in order to prevent any further growth. A paraformaldehyde (PFA) solution was used to fix cells at specific time points. The scaffold was removed from the media and placed in a new well with PBS. The PBS was then removed and replaced with 200 μL of 4% PFA solution. This was then incubated for 20 minutes at RT and washed with PBS. The fixed cells were then stored in 500 μL PBS at 4°C.

Cell morphology staining

The two stains used in the study were phalloidin to stain the actin filaments of the cells and DAPI to stain the nuclei. The phalloidin stock solution (Alexa Fluor™ 594 Phalloidin, Invitrogen) was prepared by dissolving the provided powder in 150 µL DMSO to yield a 400x stock solution. A working solution was prepared by using 0.5 µL of this stock in 200 µL PBS for every sample stained. A working solution of DAPI (Thermo Scientific) was prepared using 0.2 µL stock solution in 200 µL PBS for every sample stained. To stain the cells, a 0.1% working solution of Triton X-100 was prepared in order to remove the fixation caused by PFA. 200 µL of this working Triton X-100 solution was then added to each well and incubated at room temperature for 15 minutes. All samples were then washed twice with PBS. To each well, 200 µL of phalloidin working solution was added and incubated for 30 minutes. 200 µL of DAPI was added to each well at the 25-minute mark and left to incubate until the 30-minute mark. The samples were then washed twice with PBS before imaging using a Zeiss confocal SP3 microscope. For long term storage, a few drops of antifade mounting media (ProLong, Invitrogen) were added and samples were stored at 4 °C protected from light.

MTT assay

MTT was purchased from Sigma Aldrich and mixed with PBS to create a stock solution of 5 mg/ mL. This solution was filtered with a 22 µm pore filter under sterile conditions so that it could be combined with media for use in cell culture. To conduct the MTT assay, two different procedures were performed depending on if the analysis was conducted on a well with just cells or a well with a scaffold. For wells with only cells, 200 µL of the stock solution was added and mixed slightly by moving the plate in a figure-eight. To wells with a scaffold, a working solution of 1 mg/ mL was created by combining 1 mL of media with 200 µL of MTT stock solution for

every scaffold. The scaffolds were moved to a new well and covered with 1.2 mL of the working solution. The MTT assay was left to sit in the incubator for 3 hours. After this time, the formed formazan crystals were dissolved in 330 μL IPA. For wells containing scaffolds, the IPA was placed into a microcentrifuge tube to which the scaffold was added. For wells without scaffolds, the existing media was aspirated while not disturbing the deposited cells and crystals. The wells were washed first with 200 μL of IPA, followed by 130 μL of IPA to ensure all the crystals were dissolved and retrieved into the microcentrifuge tube. This is vital because the colorimetric analysis is very sensitive, so anything left behind in the wells or on the scaffold could dramatically alter the results.

To prepare the samples for the colorimetric analysis, each microcentrifuge tube was centrifuged at 10,000 rpm for 6 minutes to separate out the cells/ cell debris from the solution. 100 μL of this solution pipetted in duplicate into a 96 well plate for each sample. The absorbance was taken at 570 nm using SpectraMax iD3 (Molecular Devices, USA). This data was then corrected by subtracting out the absorbance of plain IPA as a blank and each duplicate was averaged together.

Results and Discussion

Despite the challenges faced with any cell seeding on a 3D structure, cell growth was observed throughout this study. Cells were able to attach and grow on both designs of coated and non-coated scaffolds, demonstrating preliminary success in cell seeding onto a 3D structure. The two different designs of scaffolds prepared, boxed pores and triangle pores, were used to align with the previous pHEMA experiments (box) and to provide an example of a more complex scaffold (triangle) for comparison in cell seeding. All scaffolds were pretreated with NaOH to assist with the hydrophobic nature of PCL before coating with pHEMA. Only benchtop pHEMA

coatings were used for cell culture due to complications in performing the agitation coatings in sterile conditions. Simple cell behaviors such as attachment and growth could be readily observed due to the GFP label encoded in the cells, resulting in fluorescent character without the use of additional assays or stains. A key finding from the cell seeding process was the improved cell attachment rates with the inclusion of the scaffold-drum compared to those placed in direct contact with the well plate. This demonstrates a viable option for improving cell seeding efficiency overall when working with scaffolds. Overall, these initial findings demonstrated compelling argument for developing a toolbox of assessments to study cellular behaviors.

Live/-Dead Assay

A Live/-Dead was selected for assessing the biocompatibility of the pHEMA coated PCL scaffold to understand possible cytotoxicity and overall cell health in this 3D culture system. The Live/-Dead assay is a staple for cell culture analysis because it allows for easy examination of live cells, which fluoresce green, and dead cells, which fluoresce red. In order to examine this assay, scaffolds were seeded with fibroblasts, chosen for their robustness, and allowed to grow for 48 hours. Two different scaffold pore designs were chosen, box and triangle, in order to align with current practices within the field as well as future proposed studies in the lab. For each scaffold type there was also a coated and uncoated group in order to examine the contribution of pHEMA. As demonstrated in Figure 14, green fluorescence was observed in the Calcein AM samples demonstrating the presence of live cells. There is noticeable green fluorescence for cells in both the pHEMA coated samples and the non-coated samples with no noticeable background fluorescence. These results demonstrate that the live assay is working as intended, allowing for the observation of live cells without any excess reactions. In the case of EthD-1, high levels of red fluorescence can be observed all along the pHEMA coated scaffolds, indicating that the dead

assay is not reacting as intended in the presence of pHEMA. This suggests that EthD-1 is fluoresces in the presence of the pHEMA coating and the absence of dead cells.

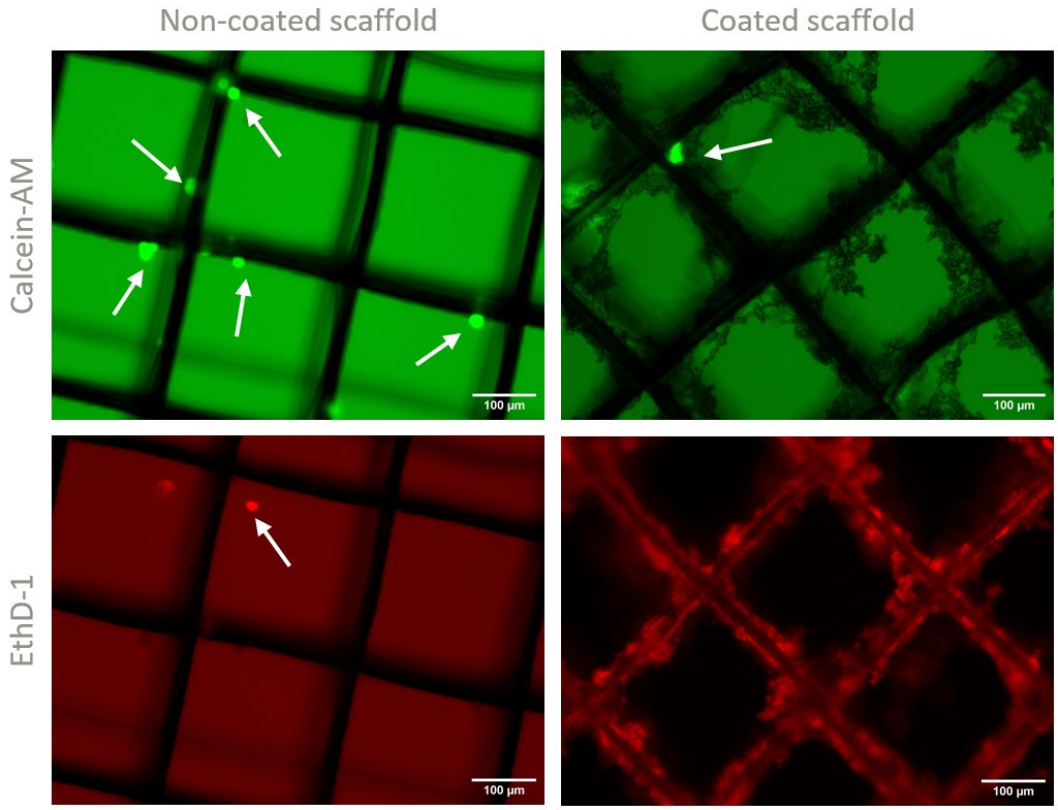

Figure 14. Results from Live/-Dead assay for non-coated and pHEMA coated scaffolds.

A Live/-Dead assay was performed after 48 hours of cell culture, white arrows point to cells. While the non-coated samples appear as expected, the high levels of EthD-1 fluorescence of the pHEMA coated sample raises a concern. Samples on the left are non-coated scaffolds, scaffolds on the right are coated in pHEMA. Imaged using an Echo Revolve microscope.

To determine if the EthD-1 was reacting to the pHEMA, additional studies were conducted by soaking scaffolds in media or PBS for 48 hours in the absence of cells. Since EthD-1 fluoresces in the presence of DNA, it is possible that exposure to factors such as the media components or cellular proteins on the hydrogel surface allowed for enough binding for detectable levels of fluorescence. The results of this study are compared to the original cell

culture findings and shown in Figure 15. With all samples displaying similar levels of fluorescence, these results indicate that the EthD-1 is reacting with the pHEMA.

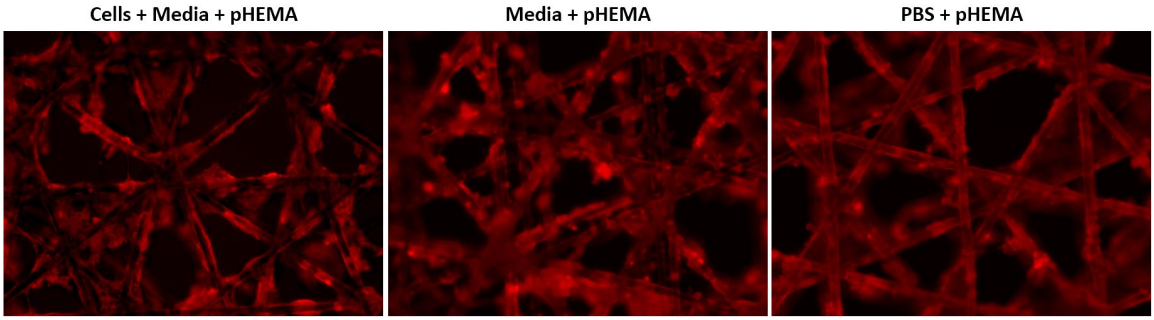

Figure 15. EthD-1 control experiments for pHEMA staining.

pHEMA coated scaffolds were prepared with three different pretreatments to determine the cause of fluorescence in the absence of dead cells. All coated scaffolds show levels of fluorescence in the presence of EthD-1. Images were taken with an Echo Revolve microscope.

These findings demonstrate that this EthD-1 is not a viable assay for pHEMA coated scaffolds. In order to determine if any dyes for dead cells could be used in the presence of pHEMA another dead stain, propidium iodine (PI), was tested. PI utilizes a similar mechanism as EthD-1 by fluorescing red when bound to exposed DNA to label dead cells. Similar to the EthD-1 control experiments, pHEMA coated scaffolds were prepared and soaked in either media or PBS. Similar to EthD-1, PI fluoresced in both conditions in the absence of any cells (Figure S4). These experiments together demonstrate that a dead cell assay is not a good fit for these pHEMA coated scaffolds due to excess fluorescence. Due to the unique structural nature of these pHEMA coatings, there is not a uniform level of fluorescence across the scaffold, making it challenging to treat it as background fluorescence in order to see if there are any dead cells in the sample. Another method for assessing cell viability would therefore be ideal when working with these coated scaffolds.

Cell morphology staining

Cell morphological stains are an important part of cell culture analysis because they allow for the assessment of the cell nuclei positioning and cytoskeleton structure. This level of understanding is critical for TE because the purpose of working in 3D systems is to better mimic cellular behaviors seen in host organisms, in particular cell morphology. The two stains used for this study were DAPI, a blue stain that binds DNA, and phalloidin, a red actin stain, due to their prevalence in literature (Hahn et al., 2019; Han et al., 2021; Jiang et al., 2021). The dyes allow for easy identification of the cell, due to the amount of DNA in the nucleus, as well as identification of the cell morphology through the actin cytoskeleton. These two colors, blue DAPI and red phalloidin, were chosen in particular since they would not fluoresce at the same wavelength as the green GFP-labeled cells. This allows for the different channels to be isolated and compared using an image analysis software such as ImageJ (Figure S5). The induced green fluorescence of the cells therefore serves as an indicator of cells when assessing if the added stains bind to anything else. Both coated and non-coated box and triangle scaffolds were prepared for cell seeding, which was conducted for 24, 48, and 72 hours. This variety in samples allowed for a large sample to ensure the pHEMA is not reacting with the stains, as well as several different cell morphologies to assess the viability of the staining method.

Across all the samples, the stains only interacted with the cells present on the scaffold demonstrating the success of this method. The stains also present as expected, with the DAPI concentrated in one location while the phalloidin stretched past this DAPI center to align with the edges of the GFP fluorescence. These results match the cellular structures these stains are meant to target, demonstrating successful cell staining. Because of the success of this staining, trends can be extrapolated from the findings shown in Figures 16-18. As seen in Figure 16,

across all the scaffold conditions there was limited spreading of the cell cytoskeletons at the 24-hour mark.

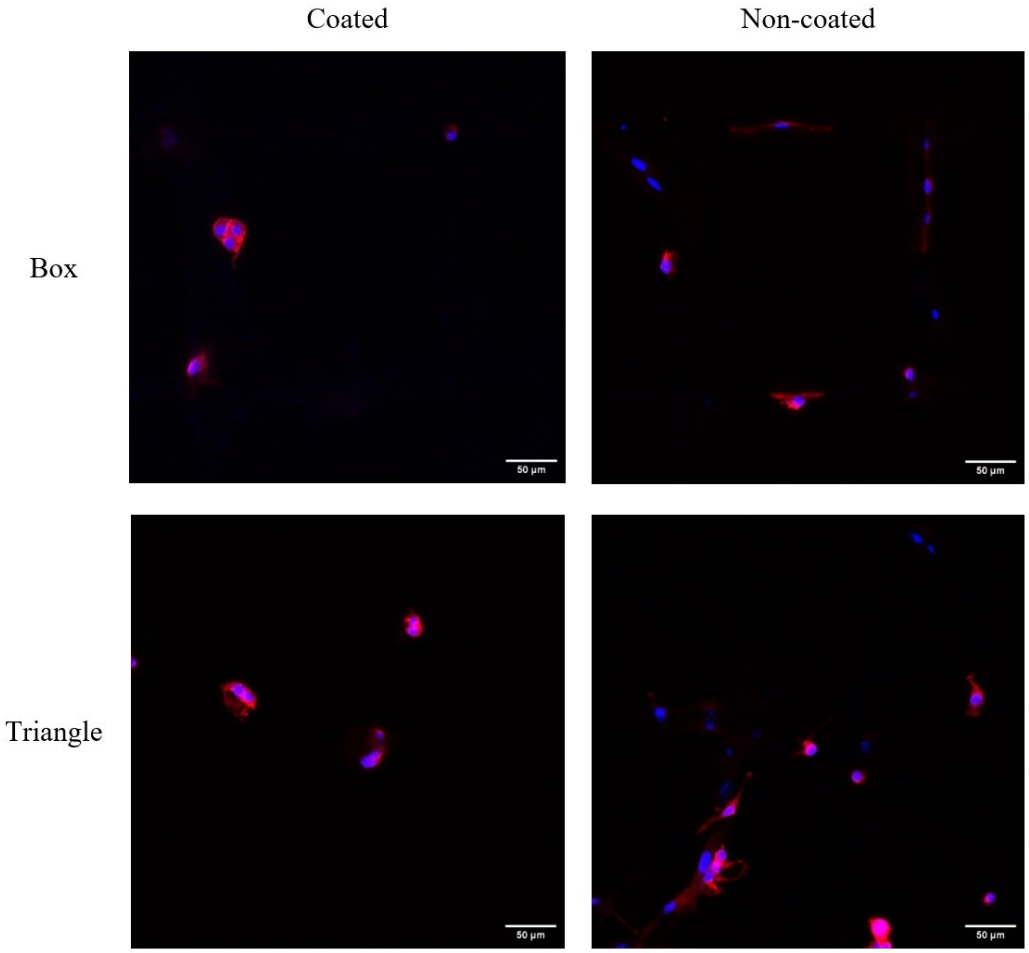

Figure 16. 24-hour cell morphology staining with DAPI and phalloidin

Scaffolds of each condition were seeded with cells that then grew for 24 hours. After this time the cells were stained with DAPI (blue) and phalloidin (red) to assess cell morphology. Scale bar 50 µm for all images.

This shifts at the 48-hour mark, Figure 17, where there is noticeable stretching of some cells, mainly in the non-coated samples. The triangle pore scaffold exhibits the most cell stretching, likely due to the increased levels of scaffold fiber interconnections and lower porosity compared to box pore scaffolds. These fibers provide a path for cellular growth as well as areas of smaller or larger gaps to bridge across.

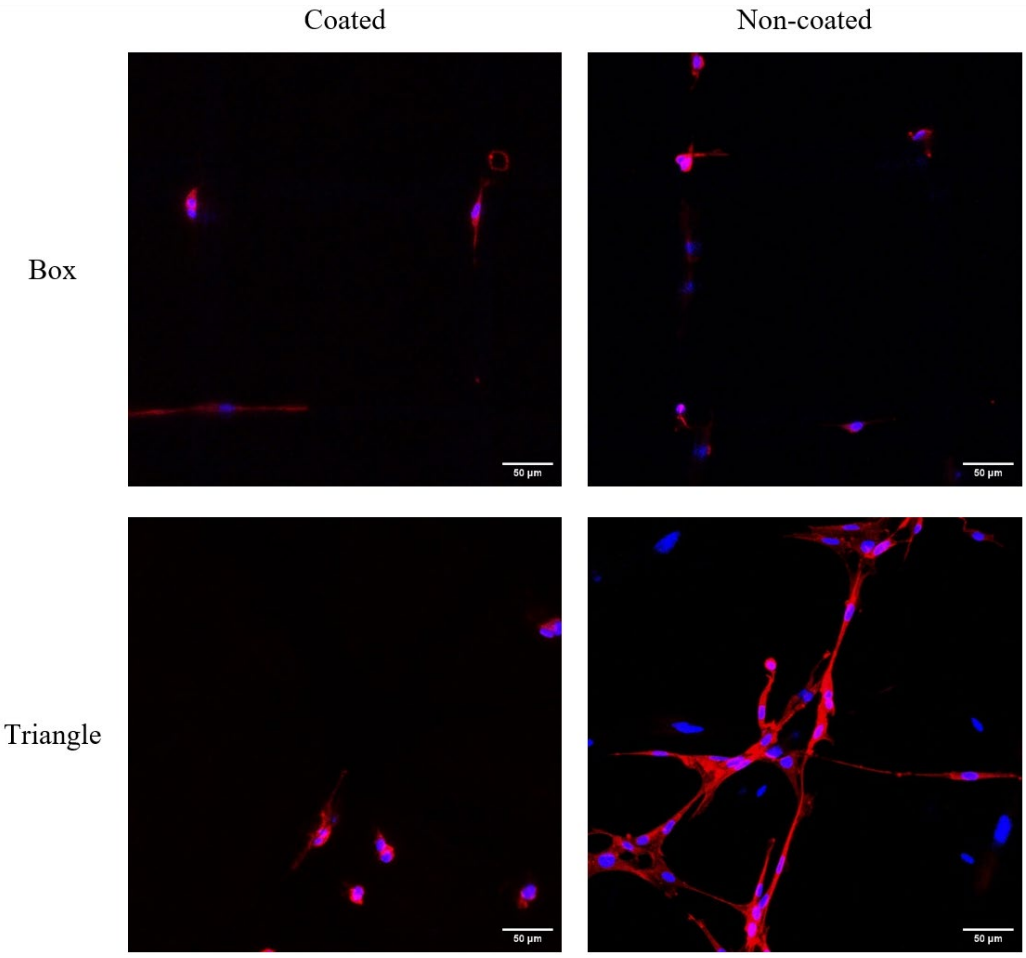

Figure 17. 48-hour cell morphology staining with DAPI and phalloidin.

Scaffolds of each condition were seeded with cells that then grew for 48 hours. After this time the cells were stained with DAPI (blue) and phalloidin (red) to assess cell morphology. Scale bar 50 µm for all images.

These trends are confirmed in the 72-hour samples, Figure 18, where the outline of the scaffold pores becomes visible in three of the four samples. While these experiments occurred over a relatively short period, by 72 hours the expected stretched morphology of the fibroblasts becomes more apparent across the samples as well as high numbers of cells clustered close together, indicating cell divisions.

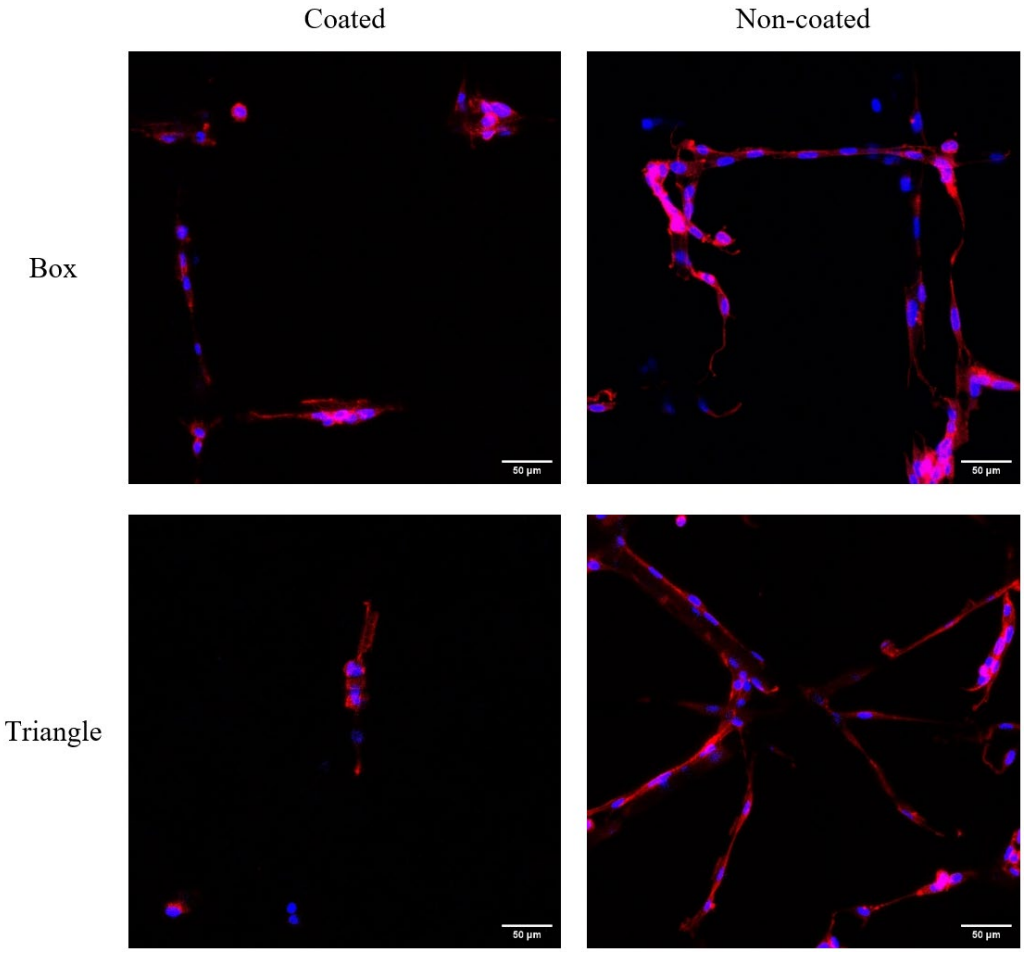

Figure 18. 72-hour cell morphology staining with DAPI and phalloidin.

Scaffolds of each condition were seeded with cells that then grew for 72 hours. After this time the cells were stained with DAPI (blue) and phalloidin (red) to assess cell morphology. Scale bar 50 µm for all images.

An important trend across the samples is the unnatural clumping of cells seen in the pHEMA coated scaffolds. This is observed at all the time points and contrasts the expected stretched morphology seen with the non-coated scaffolds. This suggests that these pHEMA coatings do not provide a conducive environment for cellular growth. Unfortunately, pHEMA does not fluoresce, so the coating structure around these cells cannot be determined through this imaging method. It is possible that these clumps of cells are due to multiple cells growing on top on a patch of pHEMA, resulting in competition for space. An alternate hypothesis is that these

cells are contained to the one area not coated by pHEMA and experiencing restricted growth from the surrounding formations and stiff polymer network. Further studies will be needed in order to determine the cause of this behavior on the coated scaffolds. Due to the limited number of results, any observed trends would need to be further investigated before any substantial conclusions could be made. Together, these results demonstrate that cell staining can be used to assess the viability of these pHEMA coated scaffolds for future experiments. This is critical because it will allow for the assessment of how the pHEMA coatings affect the cell morphology overtime compared to cells seeded on plain PCL scaffolds, in 2D well plates, and known natural structures.

MTT assay

An MTT assay provides an opportunity for assessing cell viability as well as cellular activity, making it a versatile test for one's cell culture toolbox. This assay provides information on cellular activity based on the conversion of MTT to purple crystals. This conversion occurs in the presence of an NAD(P)H dependent enzyme, making it dependent on the level of metabolic activity in the cell. If cells have a high metabolic activity, it means they are not only alive but actively growing and dividing, indicating a suitable environment (Ghasemi et al., 2021). This assay allows for valuable information regarding the suitability of the environment for cell growth and maintenance. One downfall of the assay is the high sensitivity of the colorimetric analysis. Both the pHEMA and the PCL scaffold could interfere with the formation and collection of these crystals, which would skew any results of the assay, making it an unsuitable fit for our model. To determine the viability of an MTT assay for these pHEMA coated scaffolds both of these parameters must therefore be assessed.

To first assess if the pHEMA interfered with the formation of these crystals, one of each scaffold type was used in the absence of any cells. These scaffolds were soaked in cell culture media for the same duration as typical for cell culture and then assessed with an MTT assay. These results are shown in Figure 19 and compared to a media sample without any scaffold.

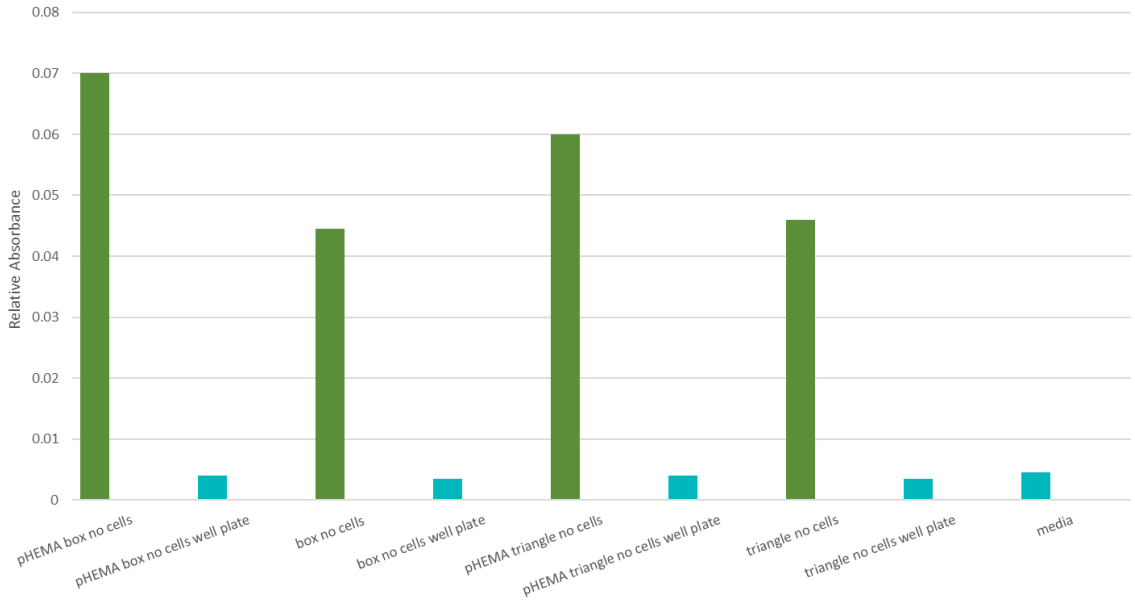

Figure 19. MTT assay results for scaffolds without cells.

MTT assay was performed at the 48-hour mark on scaffolds soaked in media with no cells to assess the interaction between MTT and the construct. Both the scaffold, shown in green, and the remaining media, shown in teal, were assayed with MTT.

In comparing the coated and non-coated scaffolds there is a slight increase in relative absorbance for coated samples. Since the overall readings from these results are an order of magnitude lower than what is seen in the presence of cells, these readings are considered negligible and non-interfering background. This demonstrates that the pHEMA coating does not substantially interfere with the mechanism of the MTT assay. The media the scaffolds were soaked in was also assessed and compared to fresh media to determine if there was anything leaching into the solution. These readings are all within a small range, demonstrating nothing was left behind in

the media. With these findings, it was determined that the pHEMA coating and the scaffolds did not substantially interfere with the MTT assay, allowing for cell studies.

Based on the findings of this control study, we investigated the cell metabolic activity on the scaffolds after 48 hours of growth. Each condition was performed in triplicate and then averaged together, with the exception of the pHEMA coated triangle pore scaffold which was conducted in duplicate due to the loss of one sample. At the 48-hour mark, the MTT assay was conducted, and the results are shown in Figure 20.

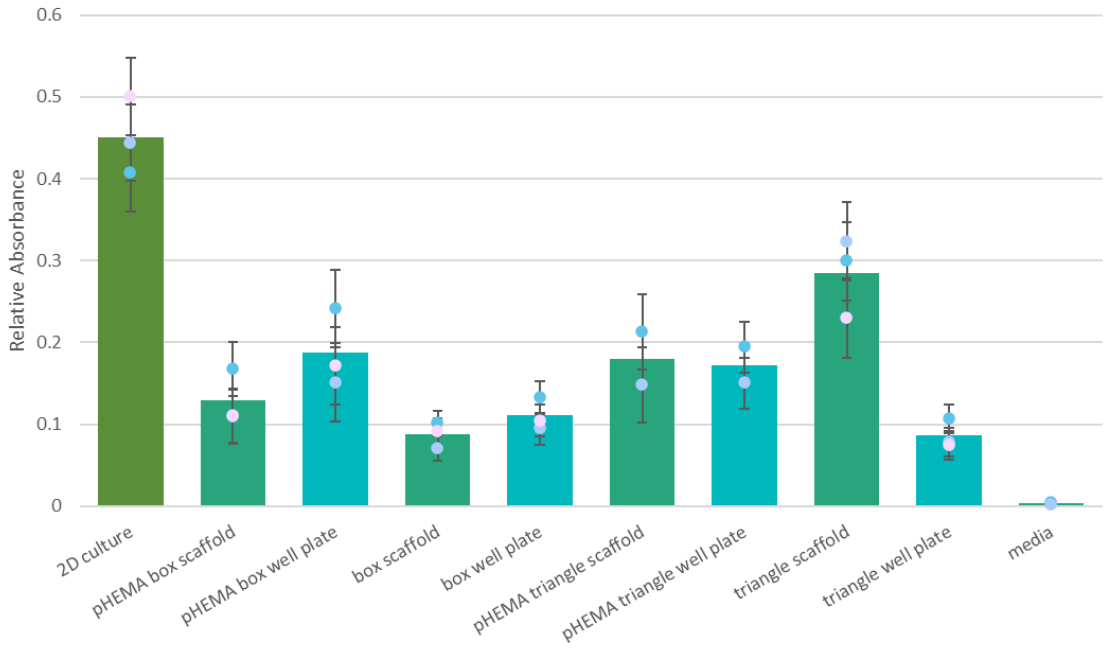

Figure 20. MTT assay results for 48-hour cell seeding.

MTT assay was performed at the 48-hour mark after cell seeding in triplicate. Both the scaffolds, shown in blue-green, and the well plate where they sat, shown in teal, were assayed for cellular activity. The 2D cell control, shown in green, was grown on the surface of the well plate. The average relative absorbance is reported with the bars as the average. The points show each absorbance ± SD (n=3).

The primary finding from this study demonstrated that approximately half of the cells seeded ended up on the bottom of the well plate, while the other half stayed on the scaffold, leading to a cell seeding efficiency of approximately 50% (Figure S6). Since the scaffolds were washed twice

as part of this process, the cells that did remain were strongly attached as well as metabolically active. These wash steps also would have stressed the cells, which could account for the lowered metabolic activity. These findings also suggested that cells were able to better attach to the triangle pore scaffold than the square pore scaffold. This was likely due to the increased number of corners present with the triangle pore scaffolds and lower porosity. These corners provide increased areas of support for cells which could promote stronger attachments or better protect the cells from washing steps. Looking at each specific condition, there are differences between each sample that could be accounted for by unsuccessful recovery of the crystals, or more likely by differences in cellular activity across triplicates. Due to the small sample size and the variable nature of cells with this high level of handling, a larger study would be needed in order to determine if these shifts are due to user error or natural variations in behavior. Visual inspection of samples determined that there were no remaining crystals on the well plate or on the scaffold, but due to the high sensitivity of colorimetric analysis this cannot be ruled out as a possibility. The final takeaway from this experiment is the relatively lower relative absorbance noted on the pHEMA coated scaffolds compared to the non-coated scaffolds. This suggests that the cells are less inclined to bind to the pHEMA, resulting in lower metabolic rates. Alternatively, is possible that the same number of cells bound to the pHEMA coated scaffolds, but are not in a suitable environment for high levels of growth and division. This motivated the final experiment, examining cell behavior over time through this MTT assay.

The final experiment consisted of examining the metabolic activity of cells seeded on these different scaffold types at 24, 48, and 72 hours in order to better understand the cell behavior in the context of these coatings. Examining the cells over this time period would allow for initial assessments of if the pHEMA coated scaffolds are able to promote cell growth as well

as further establish levels of cell attachment. The findings of this experiment are shown in Figure 21.

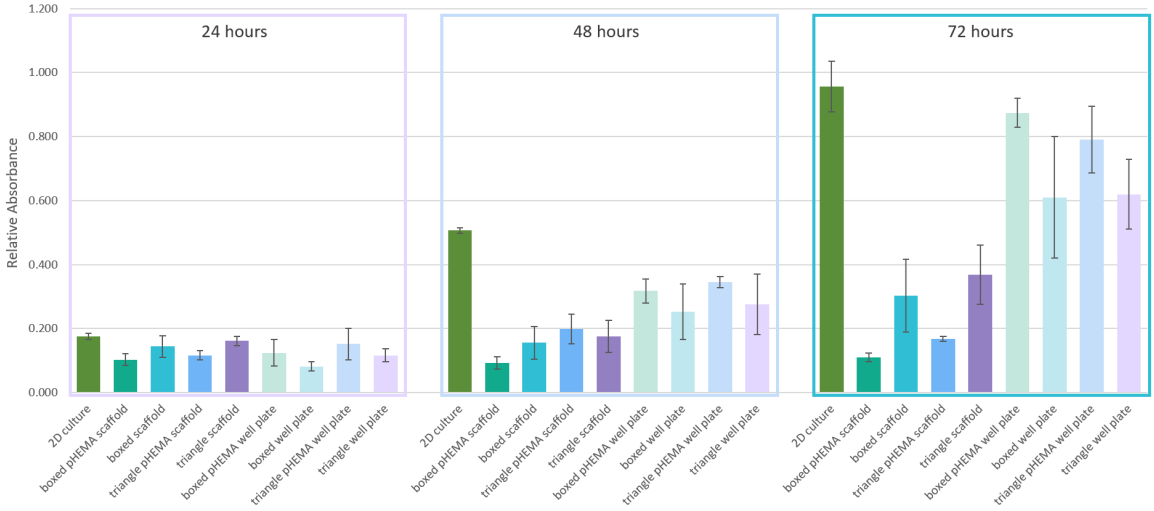

Figure 21. MTT assay results over course of three days.

MTT assays were performed on identical groups of samples at the 24, 48, and 72-hour mark. Each sample was measured both for cellular activity on the scaffold and activity of cells left in the media in the well plate. The scaffold results are shown in darker colors while the media results are shown in pastels. The cell controls were grown on the surface of the well plate. Relative absorbance represented as average ± SD (n=3).

This study suggests that cells seeded on pHEMA coated scaffolds exhibited lower levels of metabolic activity compared to the non-coated samples. The lowered activity could be accounted for by the increased cellular activity on the well plate. This could be due to the cells not adhering to the pHEMA as expected or that the pHEMA blocked desirable attachment points for the cells. Similar to the first 48-hour study, the combination of the cellular activity on the scaffold with the cellular activity in the well plate closely resembles the total cellular activity of the cell control (Figure S7). This demonstrates a consistency in cell seeding efficiency, supporting the hypothesis that the reduced cellular activity on the scaffolds is due to lack of adhesion rather than insufficient cell populations. Overall, these findings demonstrate that an MTT assay is

compatible with pHEMA coated scaffolds and can be used to determine valuable information regarding the cells in this 3D environment.

Conclusions

By constructing a toolbox of compatible cell assays for pHEMA coated scaffolds, these hybrid designs have demonstrated preliminary suitability for further TE studies. In order to assess the practicality of a clinical intervention for individuals, it must first be understood on a cellular level through the use of *in vitro* studies. These studies provide valuable information by using different types of assays to assess cell behaviors, morphology, and viability. These studies demonstrated two viable methods for assessing the relevance of pHEMA coated scaffolds for cell-based applications. While the Live/-Dead assay did not succeed due to binding and fluorescence of the pHEMA in the presence of the dead stain, there are other methods of assessing cell viability such as cytotoxicity tests that can serve in its place. Cell staining with DAPI and phalloidin provides information regarding cellular morphology which is valuable for assessing the success of a 3D culture method. The MTT assay provides valuable insights to cell metabolic activity as well as wellbeing since it assesses metabolic rates which are associated to cellular growth. Together, the success of these two assay methods provides valuable information and a suitable starting point for assessing the implementation of pHEMA coated scaffolds for TE.

In evaluating the application of these assays for pHEMA coated scaffolds, trends emerged regarding the cellular interactions. Overall, these results suggest that the pHEMA coatings do not provide an ideally conducive environment for cellular growth despite their similarity to ECM structures. In observing cell morphologies, there is both abnormal clumping and low levels of cell division on pHEMA coated scaffolds compared to non-coated scaffolds.

This is further supported by the results of the MTT study, where low levels of metabolic activity were noted on pHEMA coated scaffolds at the same time points. These results indicate that while the cells were able to attach to the scaffolds, they were not able to rapidly proliferate under these conditions. This suggests that the pHEMA contributed to an environment stressful to cellular growth, as noted by in a previous study by Lydon. Despite the hydrophilic nature of pHEMA, which has been demonstrated to aid cell attachments, the hydroxyl groups present in the polymer structure has been suggested to interfere with cell attachment (Lydon et al., 1985). Since the pHEMA in these studies was not functionalized, this hydroxyl group is still present in the polymer and could interfere with cellular attachments as Lydon demonstrates. While this complicates the implication of pHEMA for TE applications, the success of other studies using pHEMA demonstrates that it can be functionalized to support cell growth. These results demonstrate areas for further improvement as well as specialization for these hybrid constructs when working in TE.

Chapter 3: Future Directions

Based on the finding of these experiments, next steps should focus on functionalizing the pHEMA coatings to promote the desired cell attachment interactions. These types of modifications have been demonstrated through the incorporation of other polymers as well as inclusion of peptides or proteins (Dursun Usal et al., 2019; Paterson et al., 2013). Based on the findings of Lyndon et al. it is likely that this functionalization process binds the problematic hydroxyl group of pHEMA. While this does result in extra processing for successful utilization of these hybrid structures, it also provides an opportunity for increased scaffold specialization. There are many different ECM compositions throughout the body, corresponding to different cellular needs and requirements. This additional step therefore provides a method for applying these readily producible scaffolds to a variety of different applications. Future studies involving these different functionalization methods would therefore improve the application as well as the scope of uses for these scaffolds.

Supplemental Figures

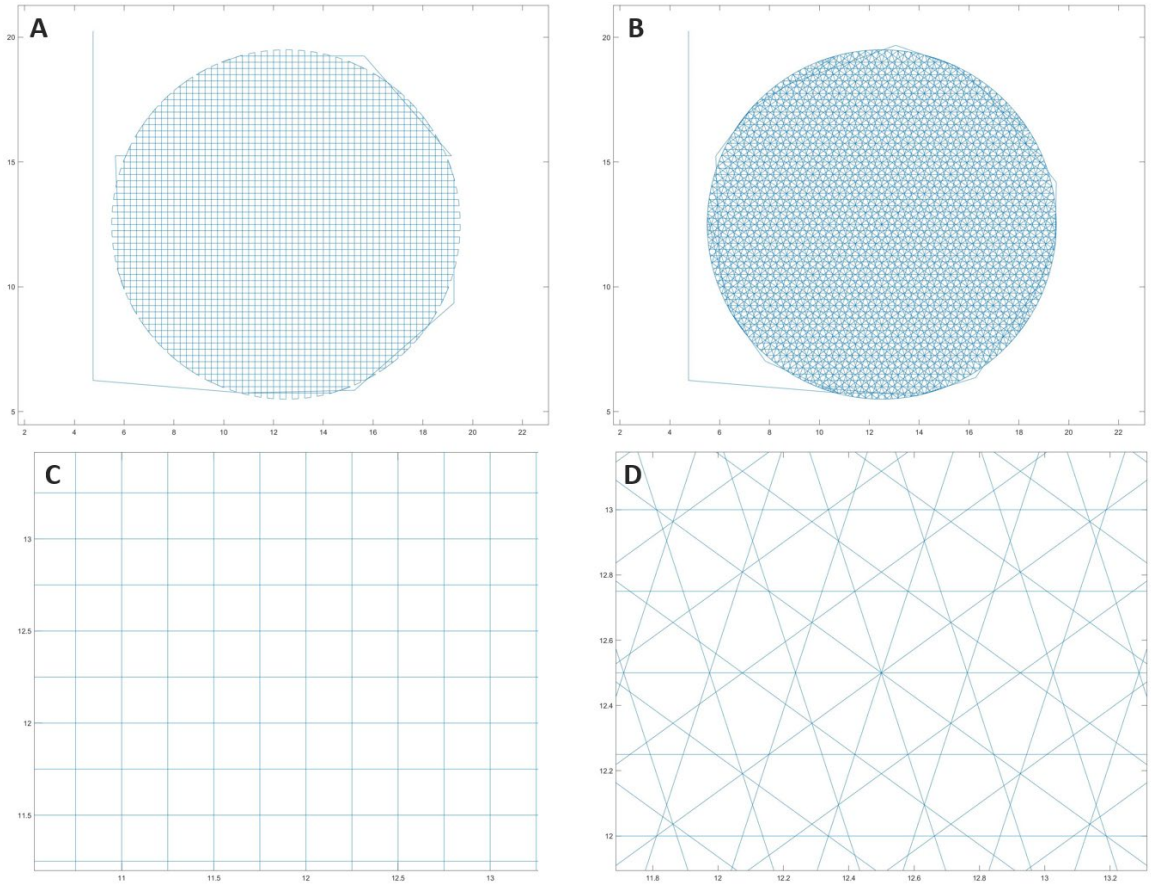

Figure S1. MATLAB generated scaffold designs.

Computer rendering of MATLAB generated scaffold design. These designs were then translated to G-code to be printed. (A) box pore full scaffold. (B) triangle pore scaffold full scaffold. (C) closeup of box pores. (D) closeup of triangle pores.

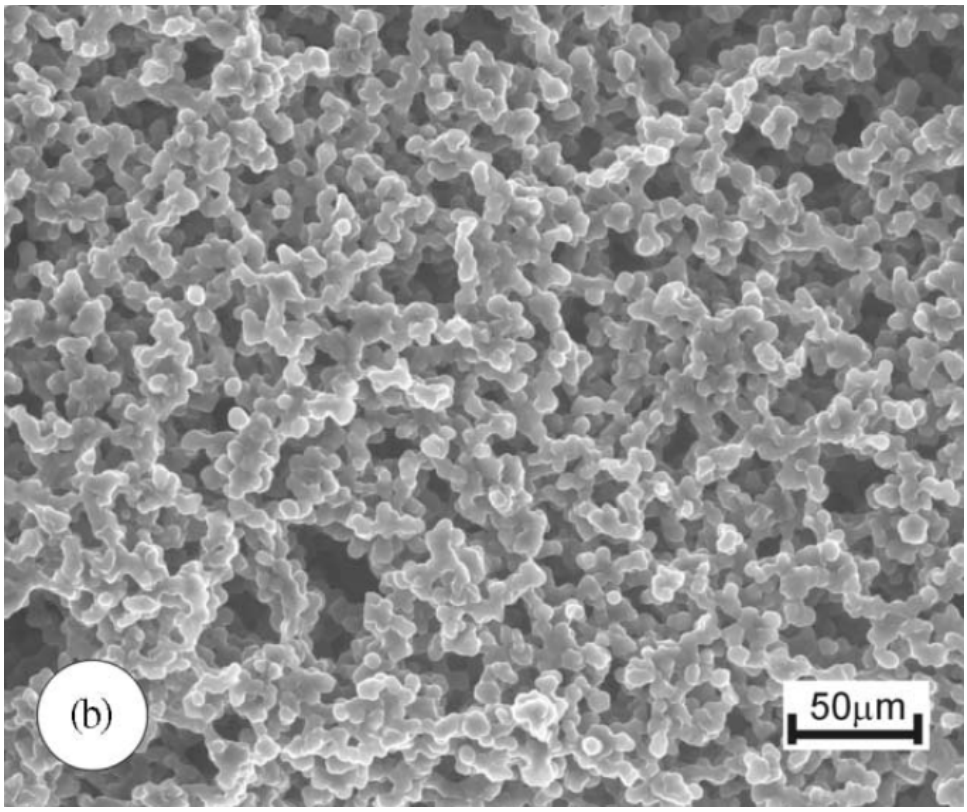

Figure S2. SEM image of pHEMA hydrogel made without PCL fibers.

High magnification of pHEMA hydrogel shows the formation of polymer spheres, contributing to the macroporous nature of the hydrogel (Dalton & Shoichet, 2001).

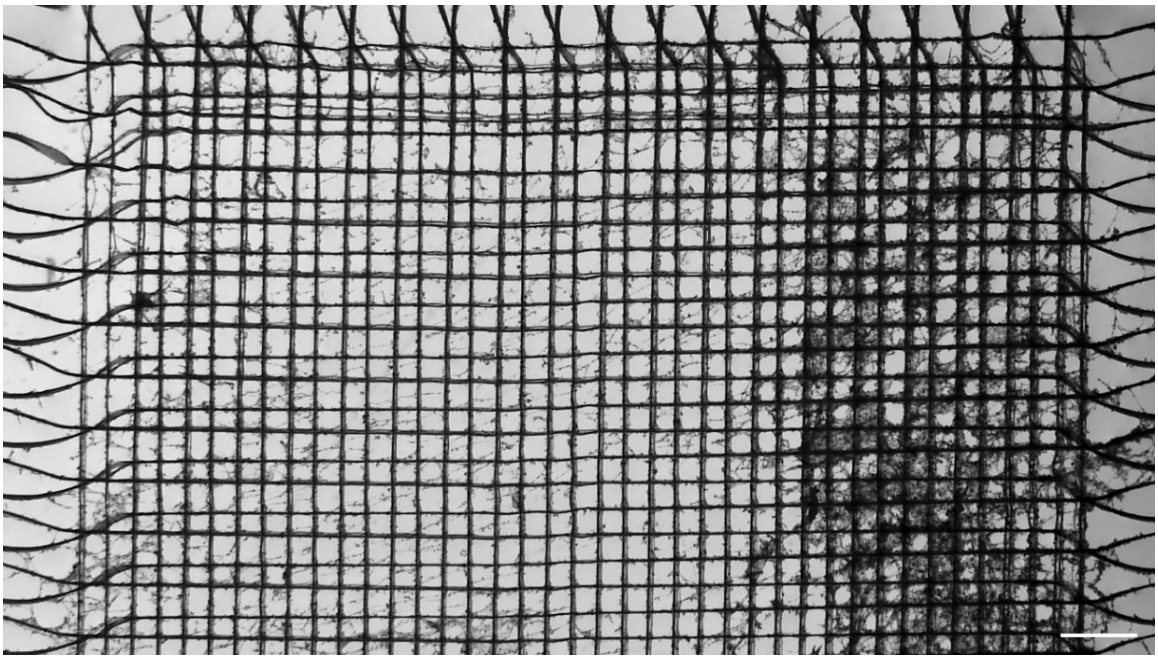

Figure S3. High speed mesh coating.

Scaffold coated with pHEMA at 201 rpm displaying a mesh coating along only the far edge.

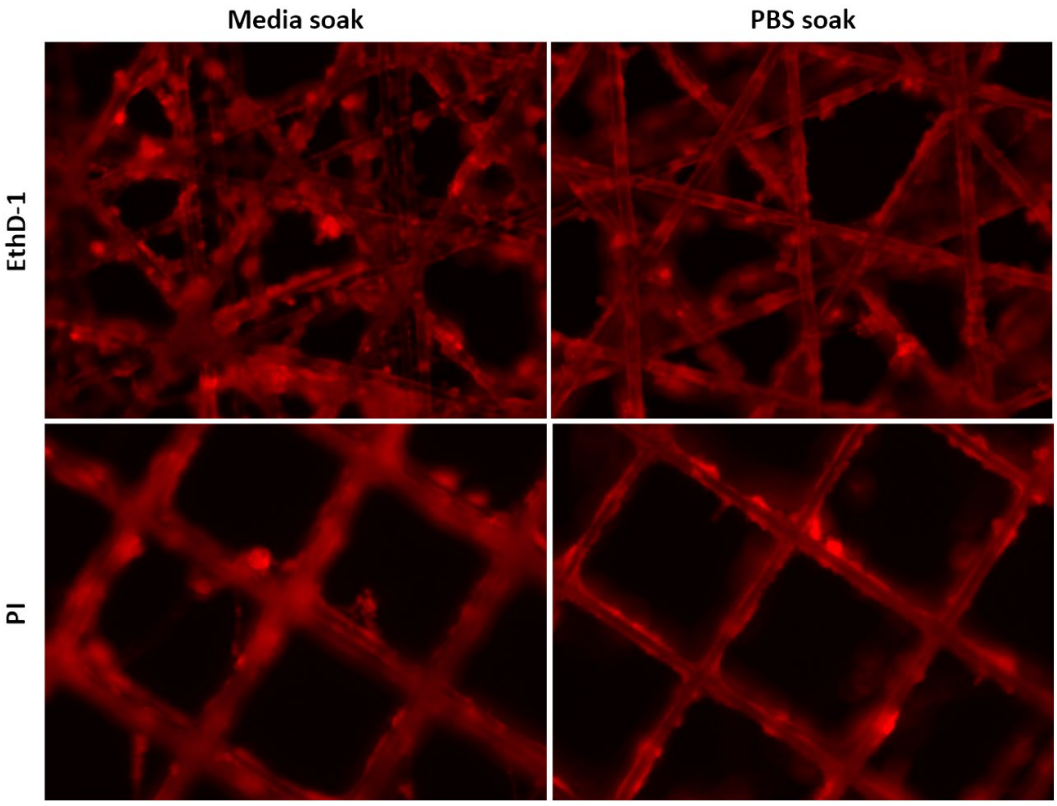

Figure S4. Comparison of different dead stains of pHEMA coated scaffolds.

pHEMA scaffolds were assayed with two different dead stains, under different soaking conditions in order to determine if pHEMA was still fluorescent. Images were taken using an Echo Revolve microscope.

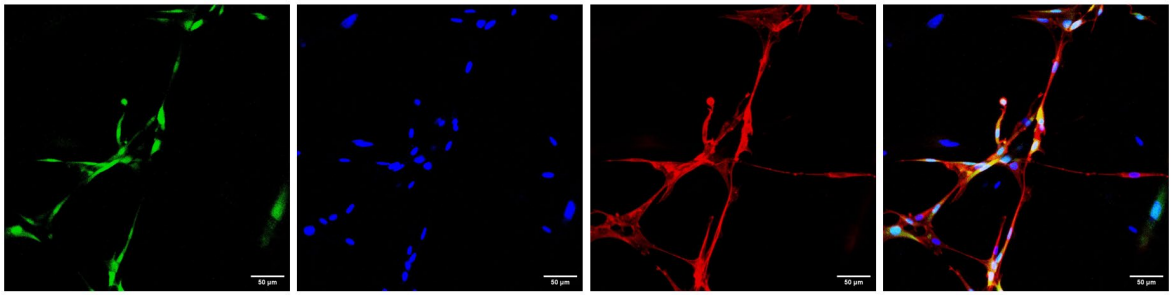

Figure S5. Channel breakdown of cell staining.

Each stain used in this study fluoresces at a different wavelength, which can then be separated for analysis. The cells are labeled with GFP (green) the nuclei are stained with DAPI (blue) and the actin cytoskeleton is stained with phalloidin (red). Scale bar of 50 μm.

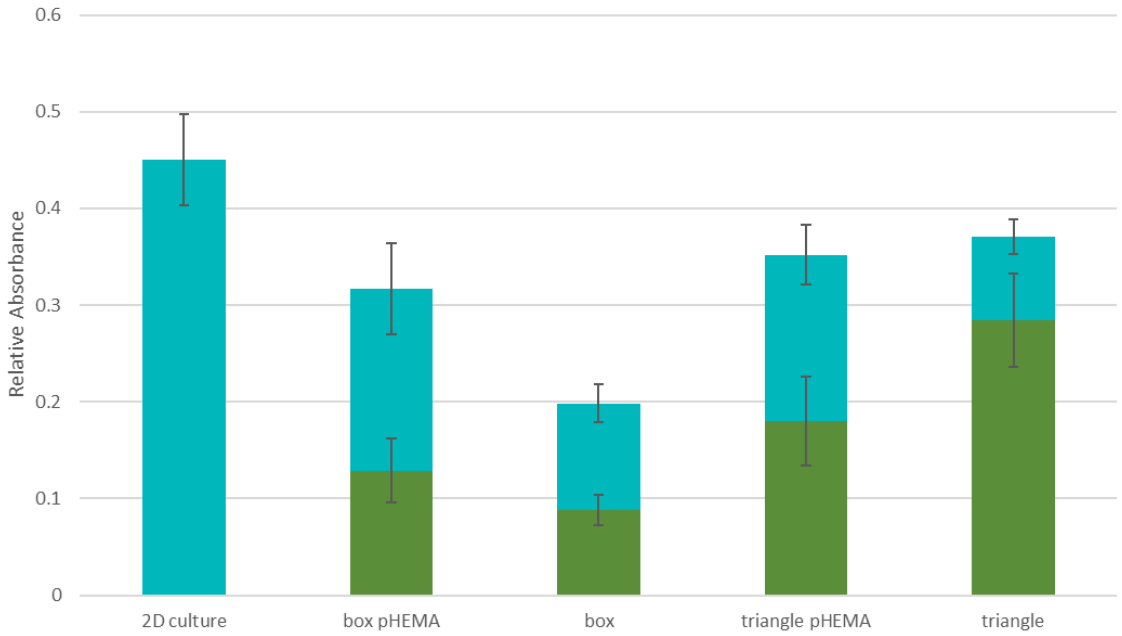

Figure S6. Stacked comparison of cell activity.

To assess the total cellular activity of cells seeded onto scaffolds, the activity on the scaffold was stacked with the activity of cells growing on the well plate. Metabolic activity of cells growing on the scaffold is shown in green, metabolic activity of cells growing on the well plate is shown in teal. Relative absorbance represented as average ± SD (n=3).

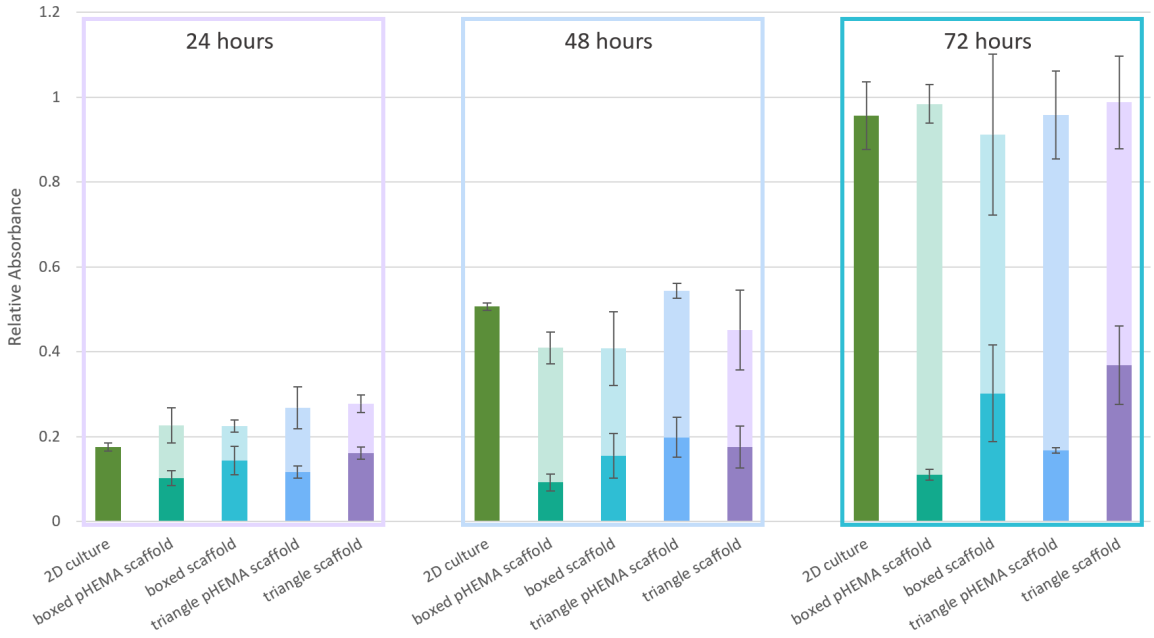

Figure S7. Stacked comparison of cell activity over three days.

To assess the total cellular activity of cells seeded onto scaffolds, the activity on the scaffold was stacked with the activity of cells growing on the well plate. Metabolic activity of cells growing on scaffolds is shown in darker colors, metabolic activity of cells grown on well plate are shown in lighter colors. Relative absorbance represented as average ± SD (n=3).

Bibliography

Abbasi, N., Hamlet, S., Dau, V. T., & Nguyen, N.-T. (2020). Calcium phosphate stability on melt electrowritten PCL scaffolds. *Journal of Science: Advanced Materials and Devices*, *5*(1), 30–39. https://doi.org/10.1016/j.jsamd.2020.01.001

Bas, O., D'Angella, D., Baldwin, J. G., Castro, N. J., Wunner, F. M., Saidy, N. T., Kollmannsberger, S., Reali, A., Rank, E., De-Juan-Pardo, E. M., & Hutmacher, D. W. (2017). An Integrated Design, Material, and Fabrication Platform for Engineering Biomechanically and Biologically Functional Soft Tissues. *ACS Applied Materials & Interfaces*, *9*(35), 29430–29437. https://doi.org/10.1021/acsami.7b08617

Bertlein, S., Hochleitner, G., Schmitz, M., Tessmar, J., Raghunath, M., Dalton, P. D., & Groll, J. (2019). Permanent Hydrophilization and Generic Bioactivation of Melt Electrowritten Scaffolds. *Advanced Healthcare Materials*, *8*(7), 1801544. https://doi.org/10.1002/adhm.201801544

Bosworth, L. A., Hu, W., Shi, Y., & Cartmell, S. H. (2019). Enhancing Biocompatibility without Compromising Material Properties: An Optimised NaOH Treatment for Electrospun Polycaprolactone Fibres. *Journal of Nanomaterials*, *2019*, e4605092. https://doi.org/10.1155/2019/4605092

Caliari, S. R., & Burdick, J. A. (2016). A practical guide to hydrogels for cell culture. *Nature Methods*, *13*(5), 405–414. https://doi.org/10.1038/nmeth.3839

Castilho, M., Hochleitner, G., Wilson, W., van Rietbergen, B., Dalton, P. D., Groll, J., Malda, J., & Ito, K. (2018). Mechanical behavior of a soft hydrogel reinforced with three-dimensional printed microfibre scaffolds. *Scientific Reports*, *8*(1), Article 1. https://doi.org/10.1038/s41598-018-19502-y

Chan, B. P., & Leong, K. W. (2008). Scaffolding in tissue engineering: General approaches and tissue-specific considerations. *European Spine Journal*, *17*(Suppl 4), 467–479. https://doi.org/10.1007/s00586-008-0745-3

Dalton, P. D., Flynn, L., & Shoichet, M. S. (2002). Manufacture of poly(2-hydroxyethyl methacrylate-co-methyl methacrylate) hydrogel tubes for use as nerve guidance channels. *Biomaterials*, *23*(18), 3843–3851. https://doi.org/10.1016/S0142-9612(02)00120-5

Dalton, P. D., & Shoichet, M. S. (2001). Creating porous tubes by centrifugal forces for soft tissue application. *Biomaterials*, *22*(19), 2661–2669. https://doi.org/10.1016/S0142-9612(01)00008-4

Daly, A. C., Prendergast, M. E., Hughes, A. J., & Burdick, J. A. (2021). Bioprinting for the Biologist. *Cell*, *184*(1), 18–32. https://doi.org/10.1016/j.cell.2020.12.002

Dash, T. K., & Konkimalla, V. B. (2012). Poly-ϵ-caprolactone based formulations for drug delivery and tissue engineering: A review. *Journal of Controlled Release*, *158*(1), 15–33. https://doi.org/10.1016/j.jconrel.2011.09.064

Dursun Usal, T., Yucel, D., & Hasirci, V. (2019). A novel GelMA-pHEMA hydrogel nerve guide for the treatment of peripheral nerve damages. *International Journal of Biological Macromolecules*, *121*, 699–706. https://doi.org/10.1016/j.ijbiomac.2018.10.060

Dzobo, K., Thomford, N. E., Senthebane, D. A., Shipanga, H., Rowe, A., Dandara, C., Pillay, M., & Motaung, K. S. C. M. (2018). Advances in Regenerative Medicine and Tissue Engineering: Innovation and Transformation of Medicine. *Stem Cells International*, *2018*, 1–24. https://doi.org/10.1155/2018/2495848

Fonseca, A. C., Melchels, F. P. W., Ferreira, M. J. S., Moxon, S. R., Potjewyd, G., Dargaville, T. R., Kimber, S. J., & Domingos, M. (2020). Emulating Human Tissues and Organs: A Bioprinting Perspective Toward Personalized Medicine. *Chemical Reviews*, *120*(19), 11093–11139. https://doi.org/10.1021/acs.chemrev.0c00342

Gao, W., Xiao, L., Wang, J., Mu, Y., Mendhi, J., Gao, W., Li, Z., Yarlagadda, P., Wu, C., & Xiao, Y. (2022). The Hollow Porous Sphere Cell Carrier for the Dynamic Three-Dimensional Cell Culture. *Tissue Engineering Part C: Methods*, *28*(11), 610–622. https://doi.org/10.1089/ten.tec.2022.0137

Ghasemi, M., Turnbull, T., Sebastian, S., & Kempson, I. (2021). The MTT Assay: Utility, Limitations, Pitfalls, and Interpretation in Bulk and Single-Cell Analysis. *International Journal of Molecular Sciences*, *22*(23), 12827. https://doi.org/10.3390/ijms222312827

Giwa, S., Lewis, J. K., Alvarez, L., Langer, R., Roth, A. E., Church, G. M., Markmann, J. F., Sachs, D. H., Chandraker, A., Wertheim, J. A., Rothblatt, M., Boyden, E. S., Eidbo, E., Lee, W. P. A., Pomahac, B., Brandacher, G., Weinstock, D. M., Elliott, G., Nelson, D., … Toner, M. (2017). The promise of organ and tissue preservation to transform medicine. *Nature Biotechnology*, *35*(6), Article 6. https://doi.org/10.1038/nbt.3889

Hahn, J., Schulze-Tanzil, G., Schröpfer, M., Meyer, M., Gögele, C., Hoyer, M., Spickenheuer, A., Heinrich, G., & Breier, A. (2019). Viscoelastic Behavior of Embroidered Scaffolds for ACL Tissue Engineering Made of PLA and P(LA-CL) After In Vitro Degradation. *International Journal of Molecular Sciences*, *20*(18), 4655. https://doi.org/10.3390/ijms20184655

Han, Y., Lian, M., Wu, Q., Qiao, Z., Sun, B., & Dai, K. (2021). Effect of Pore Size on Cell Behavior Using Melt Electrowritten Scaffolds. *Frontiers in Bioengineering and Biotechnology*, *9*, 629270. https://doi.org/10.3389/fbioe.2021.629270

Hochleitner, G., Jüngst, T., Brown, T. D., Hahn, K., Moseke, C., Jakob, F., Dalton, P. D., & Groll, J. (2015). Additive manufacturing of scaffolds with sub-micron filaments via melt electrospinning writing. *Biofabrication*, *7*(3), 035002. https://doi.org/10.1088/1758-5090/7/3/035002

Hrynevich, A., Elçi, B. Ş., Haigh, J. N., McMaster, R., Youssef, A., Blum, C., Blunk, T., Hochleitner, G., Groll, J., & Dalton, P. D. (2018). Dimension-Based Design of Melt Electrowritten Scaffolds. *Small (Weinheim an Der Bergstrasse, Germany)*, *14*(22), e1800232. https://doi.org/10.1002/smll.201800232

Jiang, Z., Zhang, K., Du, L., Cheng, Z., Zhang, T., Ding, J., Li, W., Xu, B., & Zhu, M. (2021). Construction of chitosan scaffolds with controllable microchannel for tissue engineering and regenerative medicine. *Materials Science and Engineering: C*, *126*, 112178. https://doi.org/10.1016/j.msec.2021.112178

Kade, J. C., & Dalton, P. D. (2021). Polymers for Melt Electrowriting. *Advanced Healthcare Materials*, *10*(1), 2001232. https://doi.org/10.1002/adhm.202001232

Kumar, M., & Sharma, V. (2021). Additive manufacturing techniques for the fabrication of tissue engineering scaffolds: A review. *Rapid Prototyping Journal*, *27*(6), 1230–1272. https://doi.org/10.1108/RPJ-01-2021-0011

Langer, R., & Vacanti, J. P. (1993). Tissue Engineering. *Science*, *260*(5110), 920–926. https://doi.org/10.1126/science.8493529

Löblein, J., Lorson, T., Komma, M., Kielholz, T., Windbergs, M., Dalton, P. D., & Luxenhofer, R. (2021). An initiator- and catalyst-free hydrogel coating process for 3D printed medical-grade poly(ε-caprolactone). *Beilstein Journal of Organic Chemistry*, *17*, 2095–2101. https://doi.org/10.3762/bjoc.17.136

Lydon, M. J., Minett, T. W., & Tighe, B. J. (1985). Cellular interactions with synthetic polymer surfaces in culture. *Biomaterials*, *6*(6), 396–402. https://doi.org/10.1016/0142-9612(85)90100-0

Lynch, C. R., Kondiah, P. P. D., & Choonara, Y. E. (2021). Advanced Strategies for Tissue Engineering in Regenerative Medicine: A Biofabrication and Biopolymer Perspective. *Molecules*, *26*(9), 2518. https://doi.org/10.3390/molecules26092518

Mao, A. S., & Mooney, D. J. (2015). Regenerative medicine: Current therapies and future directions. *Proceedings of the National Academy of Sciences*, *112*(47), 14452–14459. https://doi.org/10.1073/pnas.1508520112

Neves, S. C., Moroni, L., Barrias, C. C., & Granja, P. L. (2020). Leveling Up Hydrogels: Hybrid Systems in Tissue Engineering. *Trends in Biotechnology*, *38*(3), 292–315. https://doi.org/10.1016/j.tibtech.2019.09.004

Niemczyk-Soczynska, B., Gradys, A., & Sajkiewicz, P. (2020). Hydrophilic Surface Functionalization of Electrospun Nanofibrous Scaffolds in Tissue Engineering. *Polymers*, *12*(11), 2636. https://doi.org/10.3390/polym12112636

Paterson, S. M., Shadforth, A. M. A., Shaw, J. A., Brown, D. H., Chirila, T. V., & Baker, M. V. (2013). Improving the cellular invasion into PHEMA sponges by incorporation of the RGD peptide ligand: The use of copolymerization as a means to functionalize PHEMA

sponges. *Materials Science and Engineering: C*, *33*(8), 4917–4922. https://doi.org/10.1016/j.msec.2013.08.011

Paxton, N. C., Lanaro, M., Bo, A., Crooks, N., Ross, M. T., Green, N., Tetsworth, K., Allenby, M. C., Gu, Y., Wong, C. S., Powell, S. K., & Woodruff, M. A. (2020). Design tools for patient specific and highly controlled melt electrowritten scaffolds. *Journal of the Mechanical Behavior of Biomedical Materials*, *105*, 103695. https://doi.org/10.1016/j.jmbbm.2020.103695

Siddiqui, N., Asawa, S., Birru, B., Baadhe, R., & Rao, S. (2018). PCL-Based Composite Scaffold Matrices for Tissue Engineering Applications. *Molecular Biotechnology*, *60*(7), 506–532. https://doi.org/10.1007/s12033-018-0084-5

Sobacchi, C., Erreni, M., Strina, D., Palagano, E., Villa, A., & Menale, C. (2018). 3D Bone Biomimetic Scaffolds for Basic and Translational Studies with Mesenchymal Stem Cells. *International Journal of Molecular Sciences*, *19*(10), Article 10. https://doi.org/10.3390/ijms19103150

Thakur, V. K., & Thakur, M. K. (Eds.). (2018). *Hydrogels: Recent Advances*. Springer Singapore. https://doi.org/10.1007/978-981-10-6077-9

Visser, J., Melchels, F. P. W., Jeon, J. E., van Bussel, E. M., Kimpton, L. S., Byrne, H. M., Dhert, W. J. A., Dalton, P. D., Hutmacher, D. W., & Malda, J. (2015). Reinforcement of hydrogels using three-dimensionally printed microfibres. *Nature Communications*, *6*(1), Article 1. https://doi.org/10.1038/ncomms7933

Vranceanu, M., Şaban, R., Antoniac, I., Albu, M., & Miculescu, F. (2012). Development and characterization of novel porous collagen based biocomposite for bone tissue regeneration. *UPB Scientific Bulletin, Series B: Chemistry and Materials Science*, *74*, 145–156.

Youssef, A., Hrynevich, A., Fladeland, L., Balles, A., Groll, J., Dalton, P. D., & Zabler, S. (2019). The Impact of Melt Electrowritten Scaffold Design on Porosity Determined by X-Ray Microtomography. *Tissue Engineering. Part C, Methods*, *25*(6), 367–379. https://doi.org/10.1089/ten.TEC.2018.0373

Zare, M., Bigham, A., Zare, M., Luo, H., Rezvani Ghomi, E., & Ramakrishna, S. (2021). pHEMA: An Overview for Biomedical Applications. *International Journal of Molecular Sciences*, *22*(12), 6376. https://doi.org/10.3390/ijms22126376

Zhou, Z.-X., Chen, Y.-R., Zhang, J.-Y., Jiang, D., Yuan, F.-Z., Mao, Z.-M., Yang, F., Jiang, W.-B., Wang, X., & Yu, J.-K. (2020). Facile Strategy on Hydrophilic Modification of Poly(ε-caprolactone) Scaffolds for Assisting Tissue-Engineered Meniscus Constructs In Vitro. *Frontiers in Pharmacology*, *11*, 471. https://doi.org/10.3389/fphar.2020.00471